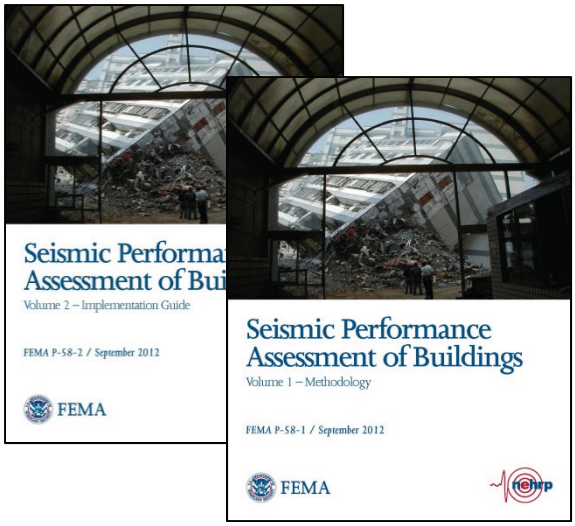

Background Document

FEMA P-58/BD-3.7.4

Simplified Response Analysis Procedures

Prepared by

Andrew S. Whittaker and Yin-Nan Huang
Department of Civil, Structural, and
Environmental Engineering
212 Ketter Hall
University at Buffalo, SUNY
Buffalo, New York 14260

Submitted to

APPLIED TECHNOLOGY COUNCIL
201 Redwood Shores Parkway, Suite 240
Redwood City, California 94065
www.ATCouncil.org

Prepared for

FEDERAL EMERGENCY MANAGEMENT AGENCY
U.S. Department of Homeland Security
500 C Street, SW
Washington, D.C. 20472

April 8, 2007

FEMA

nehrp

Background Documentation

FEMA P-58 Background Documents are a series of reports documenting the technical background and source information for key aspects of the FEMA P-58 methodology and its implementation. These reports were developed over the course of the 10-year ATC-58/ATC-58-1 Projects funded under FEMA Contracts EMW-2001-RP-0056 and HSFEHQ-06-D-1105.

Background Documents were developed by consultants, serving at various levels within the project hierarchy, reporting the results of: (1) decisions on technical development protocols; (2) focused studies on the development of key aspects of the methodology; (3) documentation of recommended procedures; and (4) collection of available data for the development of structural and nonstructural fragilities. They were initially intended to serve as a record of the technical state-of-knowledge at the time they were produced, and as resources for the development of the eventual project reports. As such, they represent a snapshot in time, and may, or may not, match the technical content, recommended procedures, or data incorporated into the final methodology and its implementation.

This Background Document is intended for the purpose of providing supplemental knowledge to users of the FEMA P-58 methodology. Information contained herein has not been independently verified for accuracy as a stand-alone document, and may have been superseded in its final implementation within the methodology. Users of information in this document assume all liability arising from such use.

Notice

Cover illustration – Primary resource documents for the FEMA P-58 *Seismic Performance Assessment of Buildings, Methodology and Implementation* series of products: FEMA P-58-1, *Volume 1 – Methodology*, and FEMA P-58-2, *Volume 2 – Implementation Guide*.

SIMPLIFIED RESPONSE ANALYSIS PROCEDURES

Introduction

The 35% draft of the ATC-58 *Guideline for Seismic Performance Assessment* (identified hereafter as the Guideline) includes simplified response analysis procedures that are based in large part on the recommendations of FEMA 440 (FEMA 2005). The analysis procedures can be used to estimate median nonlinear story drift and peak floor acceleration given spectral demands and rudimentary knowledge of the structural system.

A study is being performed to confirm the utility of the simplified procedures using nonlinear response-history analysis and lumped parameter models of sixteen buildings designed in accordance with the 2003 NEHRP Recommended Provisions. This note summarizes the work completed to date. The numerical models and earthquake ground motions are introduced. The procedures for peak roof-displacement, story-drift and floor-acceleration computations are described and results are presented. Correction factors for story drift and peak floor acceleration are developed by regression analysis using the ratios of demands computed by nonlinear response analysis and the simplified procedures.

Numerical models and ground motions

Table 1 lists the nine buildings used in this study: reinforced concrete shear walls, steel eccentrically braced frames and steel moment frames and 3-, 5- and 9-stories in height for each type of frames. The first mode periods of the buildings range between 0.18 second (3-story shear wall) and 2.55 seconds (9-story moment frame). Robust lumped-parameter stick models of these buildings were developed by Burgos (2006) for the purpose of assessing the seismic performance of different lateral force resisting systems. The Burgos models are used in this study. Bilinear hinges with 3% post-yield stiffness were assigned to all frame elements in the lumped parameter models for the nonlinear response-history analysis.

Response-history analysis was performed using two bins of earthquake ground motions, one near-fault (Bin 1) and one far-field (Bin 2), which were assembled for the ATC-58 ground-motion studies (Huang et al. 2006). Tables 2 and 3 list the 25 pairs of seed ground motions in each bin. To achieve a wide range of shaking intensity, the ground motions in Bins 1 and 2 were amplitude-scaled by 0.1, 0.5, 1 and 2 and designated as Bins 1_10, 1_50, 1_100, 1_200, 2_10, 2_50, 2_100 and 2_200, respectively. Figures 1a and 1b present the spectra for the ground motions in Bins 1_100 and 2_100, respectively. Figures 1c and 1d present median spectra for the eight bins of motions.

Acceleration, displacement and drift notation

Figure 2 defines the floor and story numbers. The floor at the base of the building is designated as Floor 1 (ground) and the roof of the building is identified as Floor N+1. The story immediately above Floor i is Story i. We used the following notation for peak floor acceleration, peak roof displacement and peak story drift:

a_i^{in} Total floor acceleration at Floor i calculated by response-history analysis.

a_i^{si} Total floor acceleration at Floor i estimated by the simplified procedure before correction.

a_i^{si*} Total floor acceleration at Floor i estimated by the simplified procedure after correction.

δ_r^{in} Roof displacement (with respect to the base of the building) calculated by response-history analysis.

δ_r^{si} Roof displacement (with respect to the base of the building) estimated by the simplified procedure.

Δ_i^{in} Drift in Story i (relative displacement of Floor i and Floor $i+1$) calculated by response-history analysis.

Δ_i^{si} Drift in Story i (relative displacement of Floor i and Floor $i+1$) estimated by the simplified procedure before correction.

Δ_i^{si*} Drift in Story i (relative displacement of Floor i and Floor $i+1$) estimated by the simplified procedure after correction.

Roof- and story-drift computations

A pseudo lateral load, *V*, for each ground motion in Bins 1 and 2 was used to compute story drifts. The load *V* was computed using:

$$V = C_1 C_2 S_a(T_1) W_1 \tag{1}$$

where $S_a(T_1)$ is the 5% damped spectral acceleration at the fundamental period of the building in the direction under consideration; W_1 is the first modal weight of the building but cannot be taken as less than 80% of total weight, *W*; C_1 is an adjustment factor for inelastic displacements; and C_2 is an adjustment factor for cyclic degradation. Coefficients C_1 and C_2 are described in FEMA 440 and the 35% draft of the Guideline. Since strength and stiffness degradation were not considered in this study, C_2 was set to be 1 for the calculation of story drifts.

The pseudo lateral force, *V*, was distributed over the height of the building with the lateral load at floor level *x*, F_x, given by:

$$F_x = C_{vx} V \tag{2}$$

using the vertical distribution factors, C_{vx} :

$$C_{vx} = \frac{w_x h_{x-1}^k}{\sum_{i=2}^{N+1} w_i h_{i-1}^k} \tag{3}$$

where w_i (w_x) is the lumped weight at Floor *i* (*x*); h_{i-1} (h_{x-1}) is the height above the effective base of the building to Floor *i* (*x*) as shown in Figure 2; and *k* is equal to 2.0 for a first mode period greater than 2.5 seconds and equal to 1.0 for a first mode period less than or equal to 0.5 second. Linear interpolation was used for intermediate periods.

For a given numerical model and a given ground motion in Bins 1 and 2, floor displacements and story drifts were computed by applying F_x at each floor level and analyzing the linear elastic model. These drifts are compared with the results of nonlinear response-history analysis to evaluate the utility of the simplified procedure.

Results for roof drift (displacement)

Figure 3 presents a statistical interpretation of results for $\delta_r^{si} / \delta_r^{in}$ and Bin 1 motions. μ and R are given by

$$\mu = \frac{\delta_r^{in}}{\delta_y} \tag{4}$$

$$R = \frac{S_a(T_1, \xi_1)W}{V_{y1}} \tag{5}$$

where δ_y is the yield roof displacement; V_{y1} is the estimated story yield strength at the effective base of the building; $S_a(T_1, \xi_1)$ is the spectral acceleration at the fundamental period and damping ratio of the building for the ground motion used for analysis and W is the reactive weight of the building. Values of δ_y and V_{y1} were established for each building using pushover (nonlinear static) analysis.

A value for $\delta_r^{si} / \delta_r^{in}$ was generated for each model and ground motion. All values of $\delta_r^{si} / \delta_r^{in}$ for Bins 1_10, 1_50, 1_100 and 1_200 and Models 1 through 9 were assembled for further analysis, except for those values associated with μ and/or R greater than 10 that were set aside. The values of $\delta_r^{si} / \delta_r^{in}$ were binned by model number, T_1 , μ and R . Values of the displacement ratio were assumed to be lognormally distributed. The 84th, 50th (median) and 16th percentiles of the displacement ratio are presented in Figure 3 as a function of model number, T_1, μ and R. The analysis was repeated for Bins 2_10, 2_50, 2_100 and 2_200 and the results are presented in Figure 4. The results show that the simplified procedure provides an unbiased estimate of median roof displacement for the 3-story and 5-story buildings. The median values of $\delta_r^{si} / \delta_r^{in}$ for the 9-story buildings are between 1.0 and 1.15 for NF motions and between 1.1 and 1.15 for FF motions.

The simplified procedure estimates the median roof displacement neutrally or conservatively (up to 15%) except for values of μ and R greater than 6 for both NF and FF ground motions. We do not consider this observation to limit the utility of the results because the simple bilinear models assumed for analysis are likely inappropriate for moderate and high values of system ductility. The dispersion is very small if μ (or R) is smaller than 1 (i.e., elastic response).

Story-drift computations

A value for $\Delta_i^{si}/\Delta_i^{in}$ was generated for each model, story and ground motion. Only values associated with μ and/or R smaller than 10 were included in the analysis. Figures 5, 6 and 7 present results for $\Delta_i^{si}/\Delta_i^{in}$ for the 3-story, 5-story and 9-story buildings, respectively, and Bin 1 motions. The 84th, 50th (median) and 16th percentiles of the displacement ratio are presented as a function of story number. The analysis was repeated for the Bin 2 motions and results are presented in Figures 8, 9 and 10.

The simplified method captures the median story drifts for eccentrically braced frames and special moment resisting frames, in an averaged sense, especially for the 3-story and 5-story buildings. The median values of $\Delta_i^{si}/\Delta_i^{in}$ for reinforced concrete shear wall buildings tend to increase with story number.

To develop correction factors for Δ_i^{si}, we generated the residual values, $\ln(\Delta_i^{in}/\Delta_i^{si})$, for all models, stories and ground motions associated with μ and/or R smaller than 10, and sorted the values by T_1, R, h_i/H and framing type, where h_i is the height of Floor $i+1$ above the base and H is the total height of the building—see Figure 2. Results are shown in Figure 11. Panels a, d and g present the residuals for 3-, 5- and 9-story EBF buildings as a function of T_1, R and h_i/H, respectively. The data shown in the second and third columns of Figure 11 are the residuals for the three SMRF buildings and three RCSW buildings, respectively. The variable *R* was forced to be 1 when the value calculated by (5) was smaller than 1. Each panel includes a regression curve calculated by Linear Least Squares (LLS) methods using a second-order polynomial. If the simplified method estimated the median story drifts without bias, the residuals would be independent of the regression variables with values equal to 0. The results of Figure 11 show that the residuals have a weak dependency on T_1 and a strong dependency on h_i/H for each type of framing system. The dependency on R is insignificant for the EBF and SMRF buildings. On average, the simplified procedure a) underestimates the story drift for h_i/H smaller than 0.4 or greater than 0.8 for EBF and SMRF buildings, b) underestimates the story drift for h_i/H smaller than 0.4 and overestimates the drift for h_i/H greater than 0.4 for RCSW buildings.

The regression model of (6) was used to develop correction factors for Δ_i^{si}:

$$\ln H_{\Delta i} = a_0 + a_1 T_1 + a_2 R + a_3 \frac{h_i}{H} + a_4 \left(\frac{h_i}{H}\right)^2 \qquad R \geq 1, i = 1 \text{ to N} \tag{6}$$

where i is the story number and $H_{\Delta i}$ is the story-drift correction factor for Δ_i^{si}. Equation (6) includes a constant, a linear term for each of T_1 and R and linear and quadratic terms for h_i/H based on the trends observed in Figure 11. The story drift for the simplified response analysis is computed as:

$$\Delta_i^{si*} = H_{\Delta i} \cdot \Delta_i^{si} \qquad i = 1 \text{ to N} \tag{7}$$

Coefficients a_0, a_1, a_2, a_3 and a_4 in (6) were computed by regression on the values of $\ln(\Delta_i^{in}/\Delta_i^{si})$ for each type of framing systems. Values for the three sets of coefficients are presented in rows 2, 3 and 4 of Table 4 and identified by $H_{\Delta E}$, $H_{\Delta M}$ and $H_{\Delta W}$ for EBF, SMRF and RCSW buildings, respectively.

The modified story drifts, Δ_i^{si*}, were computed using (7) for all models and all bins of ground motions for μ and/or R smaller than 10. The analysis of residuals presented in Figure 11 was repeated for $\ln(\Delta_i^{in}/\Delta_i^{si*})$; results are shown in Figure 12. The LLS regression curves in Figure 12 show clearly that the correction factors remove the bias evident in Figure 11. The ratios presented in Figures 5 through 10 were recomputed for $\Delta_i^{si*}/\Delta_i^{in}$; results are presented in Figures 13 through 18. The judge the utility of the correction procedure, compare the results shown in panels b and c of Figure 6 and Figure 14: the significant dependency of $\Delta_i^{si}/\Delta_i^{in}$ on the floor height has been removed. Most of the median values of $\Delta_i^{si*}/\Delta_i^{in}$ are between 0.9 and 1.1.

Floor-acceleration computations

Burgos (2006) performed a series of nonlinear response-history analysis for 2003 NEHRP-compliant buildings and showed that the distribution of median peak floor accelerations was constant over the height of a conventional EBF or SMRF building with a magnitude equal to the peak ground acceleration (PGA). Accordingly, we adopted PGA as the baseline acceleration estimate for peak floor acceleration:

$$a_i^{si} = PGA \qquad i = 2 \text{ to N+1} \tag{8}$$

where i is the floor number. A value for a_i^{si}/a_i^{in} was generated for each model, story and ground motion, and only values associated with μ and/or R smaller than 10 were included in the analysis. Figures 19, 20 and 21 present results for a_i^{si}/a_i^{in} for 3-story, 5-story and 9-story buildings, respectively, and Bin 1 motions. The 84th, 50th (median) and 16th percentiles of the acceleration ratio are presented as a function of story number. The analysis was repeated for the Bin 2 motions; results are presented in Figures 22, 23 and 24. The distribution of median a_i^{si}/a_i^{in} for each of the EBF and SMRF models is close to a constant value at all floor levels: an observation similar to that of Burgos (2006).

The residual analysis of Figure 11 was repeated for $\ln(a_i^{in}/a_i^{si})$. Results are presented in Figure 25. The dependency of the residuals on h_{i-1}/H is seen only in the data for the RCSW buildings. The residuals for smaller T_1 and R are greater than those for larger T_1 and R in an average sense. Most of the residuals for RCSW buildings are greater than zero because PGA underestimates the peak floor acceleration for such buildings. However, Figure 25f shows that the residuals decrease as the nonlinearity of the building increases (measured here using *R*).

The corrected peak acceleration at floor level i, a_i^{si*}, was computed using (9) and (10):

$$a_i^{si*} = H_{ai} \cdot a_i^{si} \qquad i = 2 \text{ to N+1} \tag{9}$$

$$\ln H_{ai} = a_0 + a_1 T_1 + a_2 R + a_3 \frac{h_{i-1}}{H} \qquad R \geq 1, i = 2 \text{ to N+1} \tag{10}$$

where i is the floor number; H_{ai} is the floor acceleration correction factor for a_i^{si}; and all other variables have been defined previously. The peak acceleration at the floor level corresponding to the base of the building was set equal to the peak ground acceleration. Coefficients a_0, a_1, a_2 and a_3 in (10) were computed by regression on the values of $\ln(a_i^{in}/a_i^{si})$ for each type of framing systems. Values for the three sets of coefficients are presented in rows 5, 6 and 7 of Table 4 and identified by H_{aE}, H_{aM} and H_{aW} for EBF, SMRF and RCSW buildings, respectively. Coefficient a_3 was forced to be zero for H_{aE} and H_{aM} based on evaluation of the residuals of the uncorrected ratios.

The residual analysis for Figure 25 was repeated for $\ln(a_i^{in}/a_i^{si*})$. Results are presented in Figure 26. The LLS regression curves in Figure 26 are either equal or very close to zero except those in panels d and e. The bias in panels d and e can be removed by adding a R^2 term to (10) but since the bias in the residuals was small for R less than 7, we decided not to modify (10). The computations used to generate Figures 19 through 24 were repeated for a_i^{si*}/a_i^{in} and the results are presented in Figures 27 through 32. All the median values of a_i^{si*}/a_i^{in} are between 0.9 and 1.1.

Remaining work

The last Phase 2 Part 4 task associated with the simplified response analysis procedure is the computation of analysis dispersions for story drift and floor acceleration.

References

Burgos, E. (2006). "Seismic performance of hybrid framing systems," M.Sc. thesis, Department of Civil, Structural and Environmental Engineering, University at Buffalo, July.

FEMA. (2005). *Improvement of Nonlinear Static Seismic Analysis Procedures*, Report No. FEMA 440, Federal Emergency Management Agency, Department of Homeland Security, Washington, D.C.

Huang, Y.-N., Whittaker, A. S, Deierlein, G. G., Hooper, J. D., and Merovich, A. T. (2006). "Scaling earthquake ground motion records for performance-based seismic design," *ATC-58 Project Technical Report*, Draft, Applied Technology Council, Redwood City, CA.

Table 1. Models analyzed in the study

Notation	Model name	Fundamental period T_1 (sec)	No. of stories	Lateral force resisting system
M1	e123	0.74	3	Eccentrically braced frame (EBF)
M2	m123	1.08		Special moment resisting frame (SMRF)
M3	w123	0.18		Reinforced concrete shear walls (RCSW)
M4	e15	1.05	5	Eccentrically braced frame
M5	m15	1.53		Special moment resisting frame
M6	w15	0.23		Reinforced concrete shear walls
M7	e19	1.78	9	Eccentrically braced frame
M8	m19	2.55		Special moment resisting frame
M9	w19	0.41		Reinforced concrete shear walls

Table 2. Near-fault ground motions

Designation	Event	Station	M[1]	r[1]
NF1, NF2	Kobe 1995	SAC 2/50 for Los Angeles	6.9	3.4
NF3, NF4	Loma Prieta 1989		7.0	3.5
NF5, NF6	Northridge 1994		6.7	7.5
NF7, NF8	Northridge 1994		6.7	6.4
NF9, NF10	Tabas 1974		7.4	1.2
NF11, NF12	Elysian Park 1 (simulated)		7.1	17.5
NF13, NF14	Elysian Park 2 (simulated)		7.1	10.7
NF15, NF16	Elysian Park 3 (simulated)		7.1	11.2
NF17, NF18	Palos Verdes 1 (simulated)		7.1	1.5
NF19, NF20	Palos Verdes 2 (simulated)		7.1	1.5
NF21, NF22	Cape Mendocino 04/25/92 18:06	89156 Petrolia	7.1	9.5
NF23, NF24	Chi-Chi 09/20/99	TCU053	7.6	6.7
NF25, NF26	Chi-Chi 09/20/99	TCU056	7.6	11.1
NF27, NF28	Chi-Chi 09/20/99	TCU068	7.6	1.1
NF29, NF30	Chi-Chi 09/20/99	TCU101	7.6	11.1
NF31, NF32	Chi-Chi 09/20/99	TCUWGK	7.6	11.1
NF33, NF34	Duzce 11/12/99	Duzce	7.1	8.2
NF35, NF36	Erzinkan 03/13/92 17:19	95 Erzinkan	6.9	2.0
NF37, NF38	Imperial Valley 10/15/79 23:16	5057 El Centro Array #3	6.5	9.3
NF39, NF40	Imperial Valley 10/15/79 23:16	952 El Centro Array #5	6.5	1
NF41, NF42	Imperial Valley 10/15/79 23:16	942 El Centro Array #6	6.5	1
NF43, NF44	Kobe 01/16/95 20:46	Takarazu	6.9	1.2
NF45, NF46	Morgan Hill 04/24/84 04:24	57191 Halls Valley	6.2	3.4
NF47, NF48	Northridge 1/17/94 12:31	24279 Newhall	6.7	7.1
NF49, NF50	Northridge 1/17/94 12:31	0637 Sepulveda VA	6.7	8.9

1. M = moment magnitude; r = closest site-to-fault-rupture distance

Table 3. Far-field ground motions

Designation	Event	Station	M[1]	r[1]
FF1, FF2	Cape Mendocino 04/25/92 18:06	89509 Eureka—Myrtle & West	7.1	44.6
FF3, FF4	Cape Mendocino 04/25/92 18:06	89486 Fortuna—Fortuna Blvd	7.1	23.6
FF5, FF6	Coalinga 1983/05/02 23:42	36410 Parkfield—Cholame 3W	6.4	43.9
FF7, FF8	Coalinga 1983/05/02 23:42	36444 Parkfield—Fault Zone 10	6.4	30.4
FF9, FF10	Coalinga 1983/05/02 23:42	36408 Parkfield—Fault Zone 3	6.4	36.4
FF11, FF12	Coalinga 1983/05/02 23:42	36439 Parkfield—Gold Hill 3E	6.4	29.2
FF13, FF14	Imperial Valley 10/15/79 23:16	5052 Plaster City	6.5	31.7
FF15, FF16	Imperial Valley 10/15/79 23:16	724 Niland Fire Station	6.5	35.9
FF17, FF18	Imperial Valley 10/15/79 23:16	6605 Delta	6.5	43.6
FF19, FF20	Imperial Valley 10/15/79 23:16	5066 Coachella Canal #4	6.5	49.3
FF21, FF22	Landers 06/28/92 11:58	22074Yermo Fire Station	7.3	24.9
FF23, FF24	Landers 06/28/92 11:58	12025 Palm Springs Airport	7.3	37.5
FF25, FF26	Landers 06/28/92 11:58	12149 Desert Hot Springs	7.3	23.2
FF27, FF28	Loma Prieta 10/18/89 00:05	47524 Hollister—South & Pine	6.9	28.8
FF29, FF30	Loma Prieta 10/18/89 00:05	47179 Salinas—John &Work	6.9	32.6
FF31, FF32	Loma Prieta 10/18/89 00:05	1002 APEEL 2—Redwood City	6.9	47.9
FF33, FF34	Northridge 01/17/94 12:31	14368 Downey—Co Maint Bldg	6.7	47.6
FF35, FF36	Northridge 01/17/94 12:31	24271 Lake Hughes #1	6.7	36.3
FF37, FF38	Northridge 01/17/94 12:31	14403 LA—116th St School	6.7	41.9
FF39, FF40	San Fernando 02/09/71 14:00	125 Lake Hughes #1	6.6	25.8
FF41, FF42	San Fernando 02/09/71 14:00	262 Palmdale Fire Station	6.6	25.4
FF43, FF44	San Fernando 02/09/71 14:00	289 Whittier Narrows Dam	6.6	45.1
FF45, FF46	San Fernando 02/09/71 14:00	135 LA—Hollywood Stor Lot	6.6	21.2
FF47, FF48	Superstition Hills (A) 11/24/87 05:14	5210Wildlife Liquef. Array	6.3	24.7
FF49, FF50	Superstition Hills (B) 11/24/87 13:16	5210Wildlife Liquef. Array	6.7	24.4

1. M = moment magnitude; r = closest site-to-fault-rupture distance

Table 4. Coefficients for the story-drift and floor-acceleration correction factors

H	**Frame type**	a_0	a_1	a_2	a_3	a_4
$H_{\Delta E}$	EBF	0.718	0.048	0.012	-2.644	2.090
$H_{\Delta M}$	SMRF	0.649	0.027	-0.010	-2.576	2.299
$H_{\Delta W}$	RCSW	1.123	-0.223	-0.059	-2.699	1.292
H_{aE}	EBF	0.573	-0.157	-0.089	0	0
H_{aM}	SMRF	0.695	-0.284	-0.080	0	0
H_{aW}	RCSW	0.334	0.216	-0.081	0.527	0

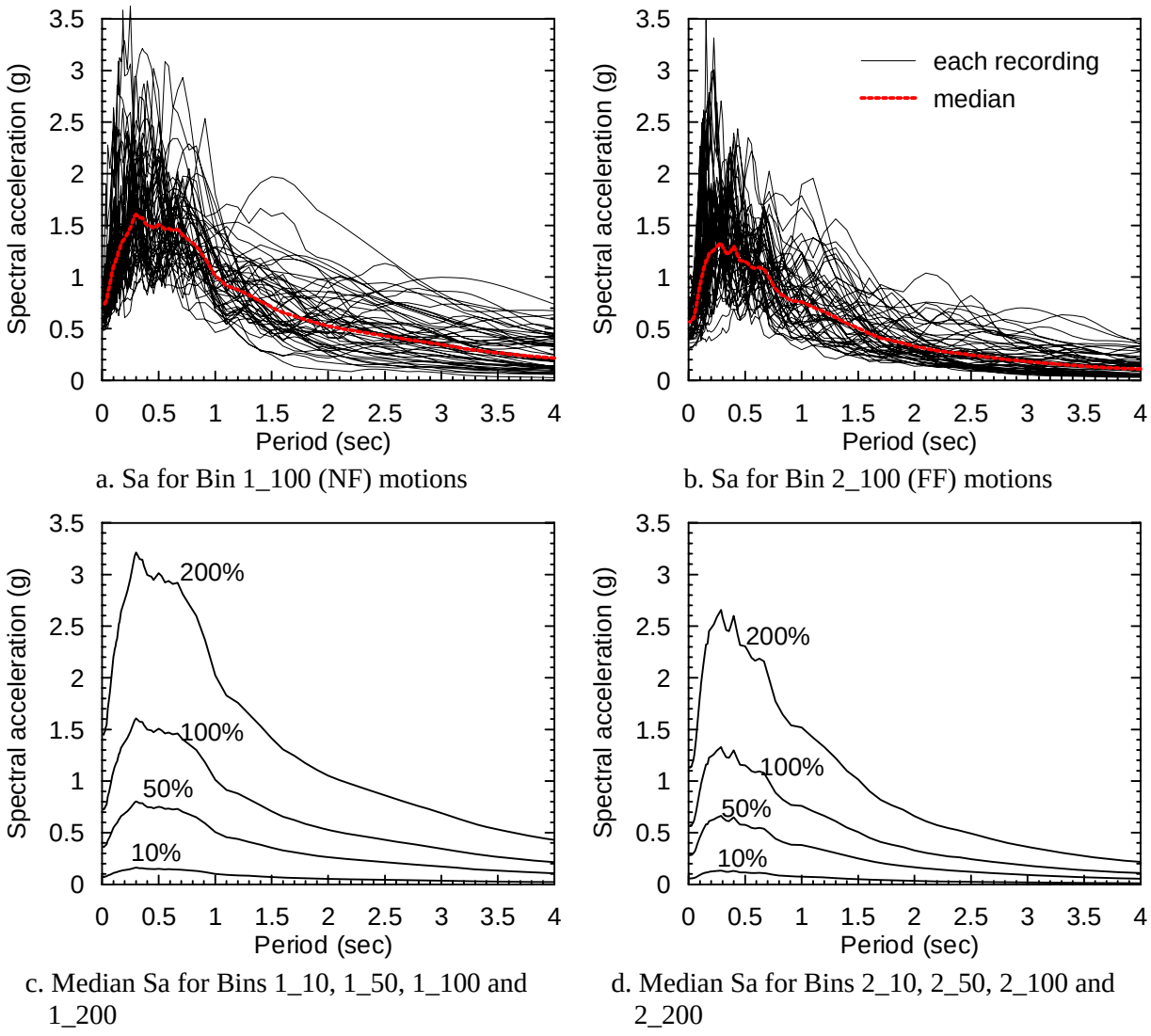

a. Sa for Bin 1_100 (NF) motions

b. Sa for Bin 2_100 (FF) motions

c. Median Sa for Bins 1_10, 1_50, 1_100 and 1_200

d. Median Sa for Bins 2_10, 2_50, 2_100 and 2_200

Figure 1. Spectral accelerations for the selected NF and FF ground motions

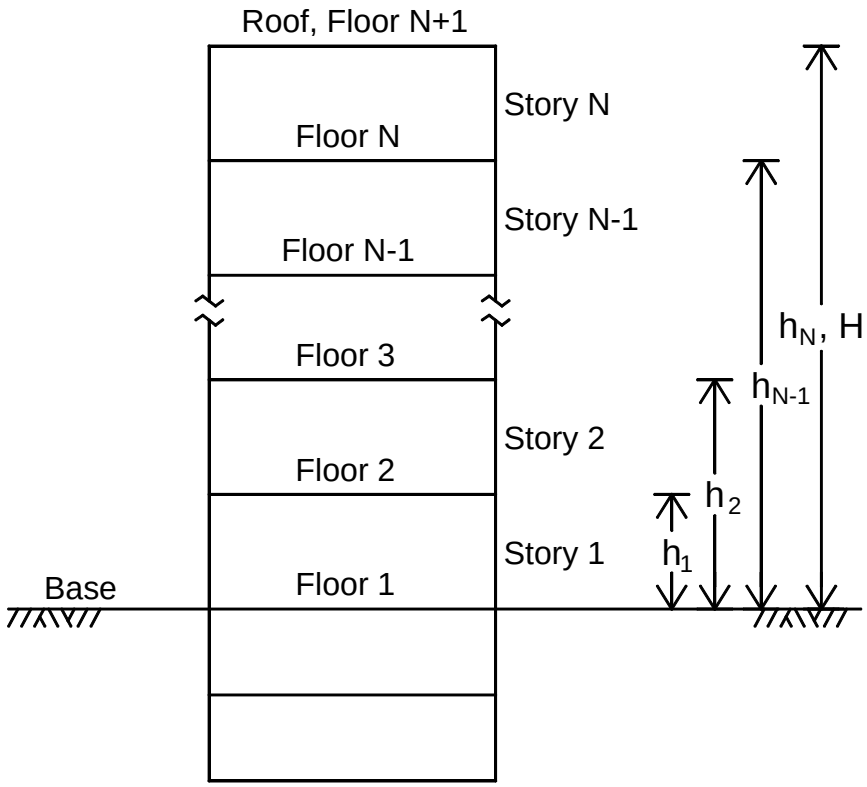

Figure 2. Floor and story numbers and computation of story height

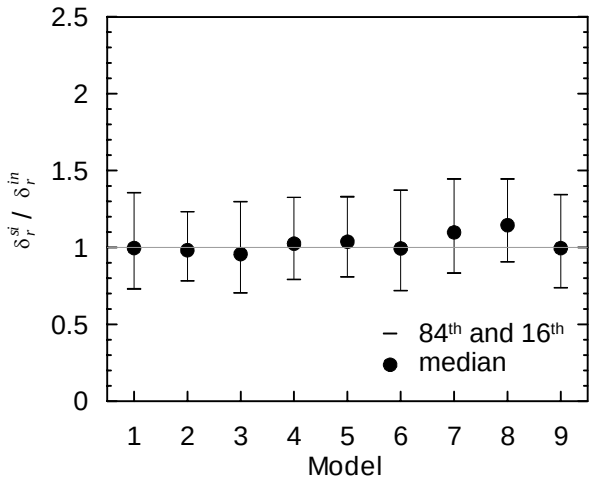

a. $\delta_r^{si}/\delta_r^{in}$ as a function of model number

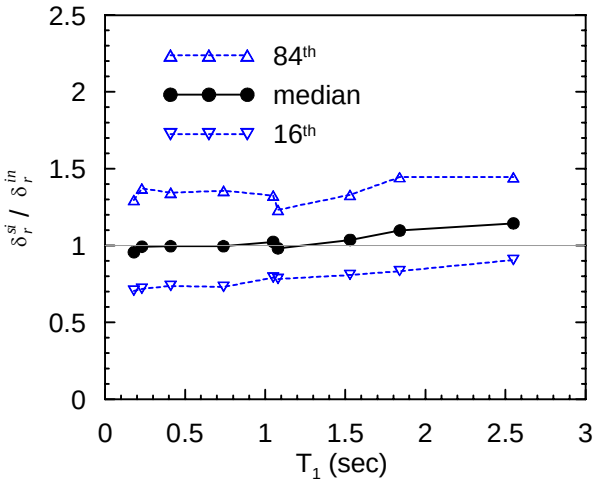

b. $\delta_r^{si}/\delta_r^{in}$ as a function of T_1

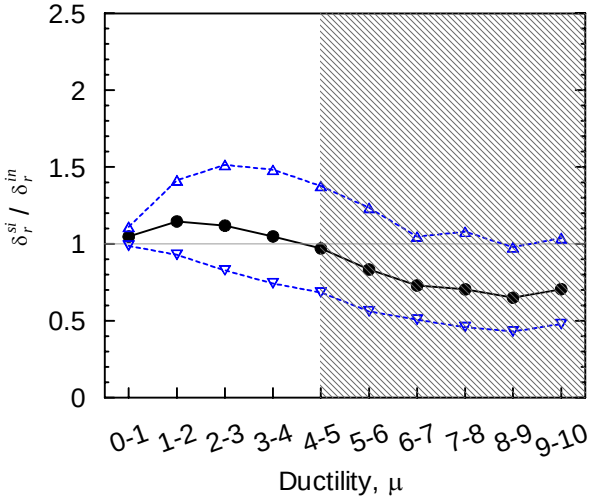

c. $\delta_r^{si}/\delta_r^{in}$ as a function of μ

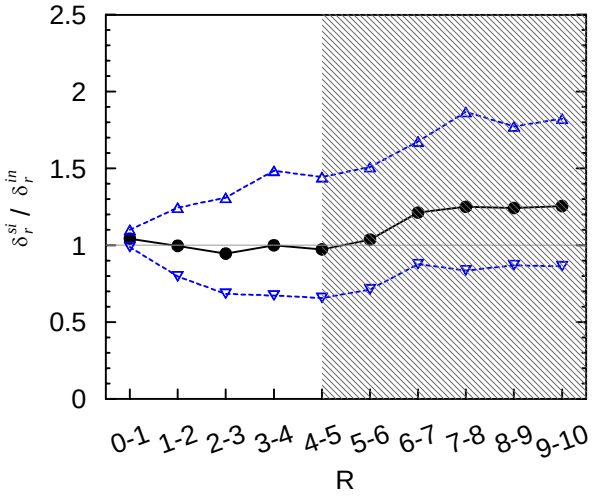

d. $\delta_r^{si}/\delta_r^{in}$ as a function of R

Figure 3. 84th, 50th and 16th percentiles of $\delta_r^{si}/\delta_r^{in}$ for NF ground motions

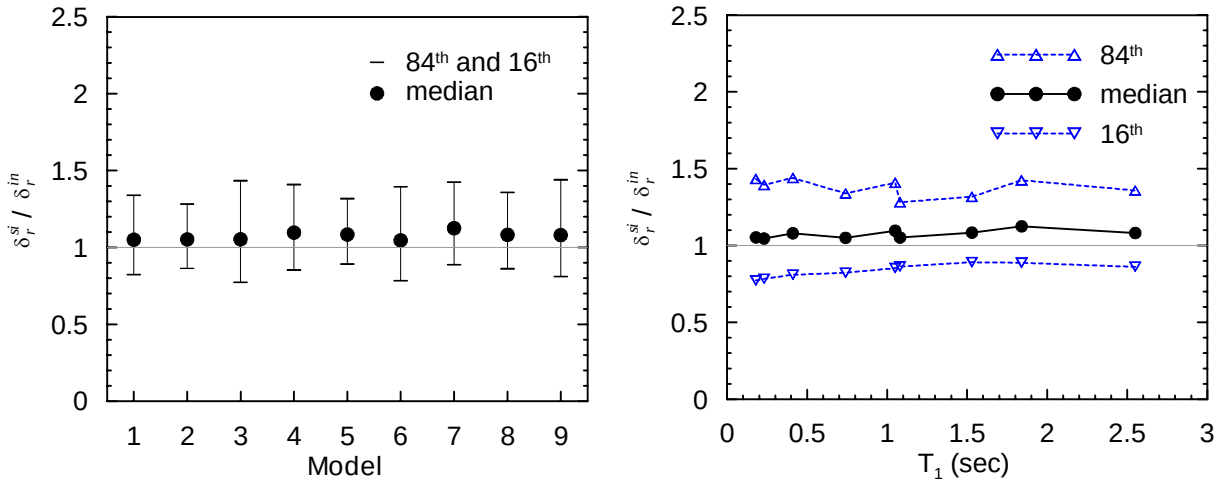

a. $\delta_r^{si}/\delta_r^{in}$ as a function of model number

b. $\delta_r^{si}/\delta_r^{in}$ as a function of T_1

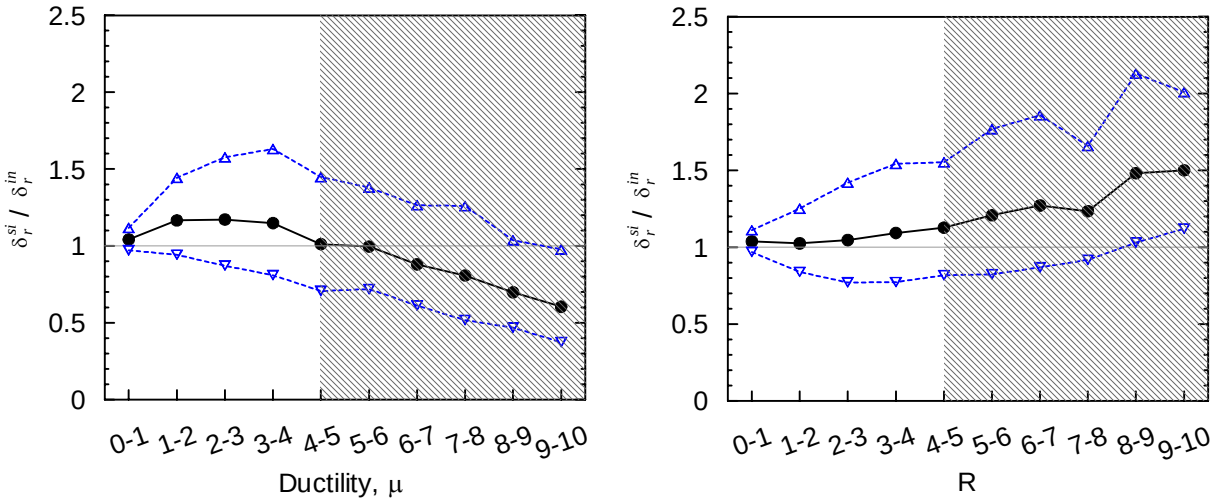

c. $\delta_r^{si}/\delta_r^{in}$ as a function of μ

d. $\delta_r^{si}/\delta_r^{in}$ as a function of R

Figure 4. 84th, 50th and 16th percentiles of $\delta_r^{si}/\delta_r^{in}$ for FF ground motions

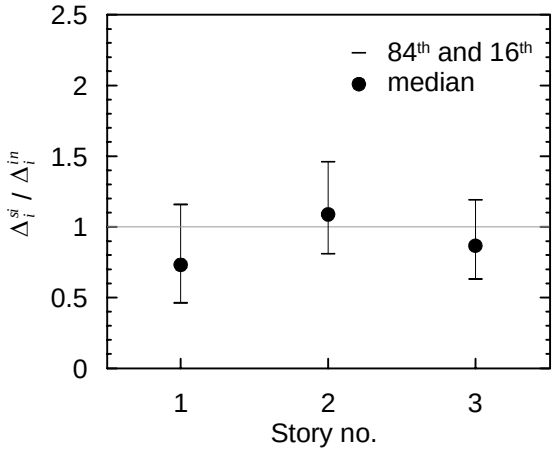

a. $\Delta_i^{si} / \Delta_i^{in}$ for M1 and NF motions

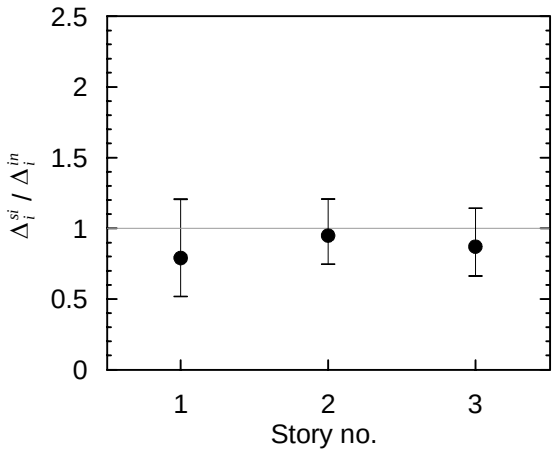

b. $\Delta_i^{si} / \Delta_i^{in}$ for M2 and NF motions

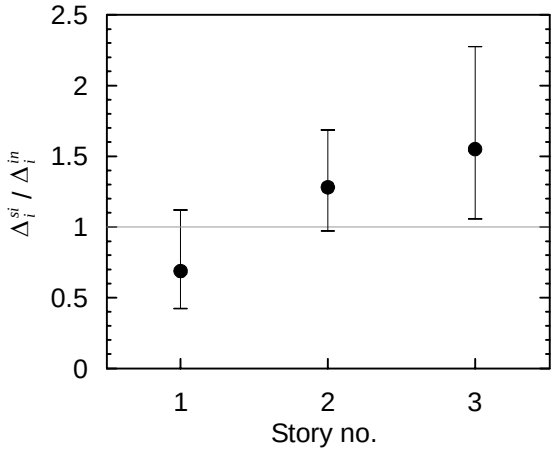

c. $\Delta_i^{si} / \Delta_i^{in}$ for M3 and NF motions

Figure 5. 84th, 50th and 16th percentiles of $\Delta_i^{si} / \Delta_i^{in}$ for three-story models and NF ground motions

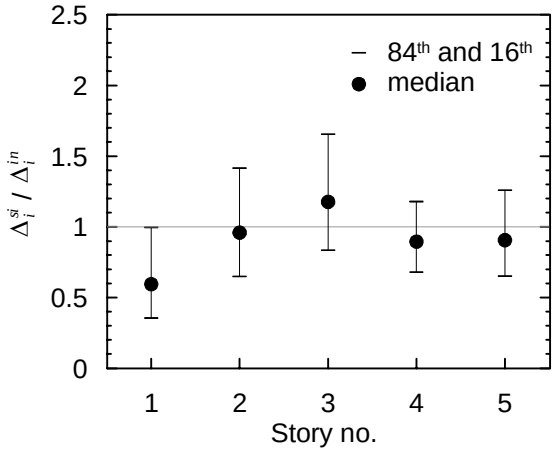

a. $\Delta_i^{si} / \Delta_i^{in}$ for M4 and NF motions

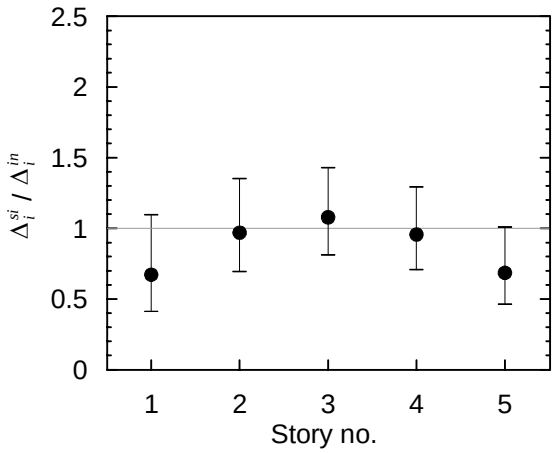

b. $\Delta_i^{si} / \Delta_i^{in}$ for M5 and NF motions

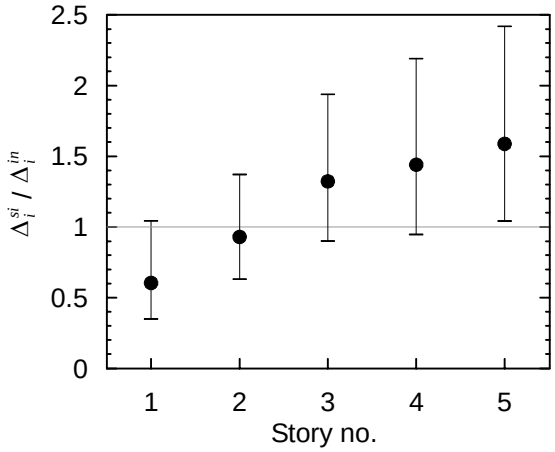

c. $\Delta_i^{si} / \Delta_i^{in}$ for M6 and NF motions

Figure 6. 84th, 50th and 16th percentiles of $\Delta_i^{si} / \Delta_i^{in}$ for five-story models and NF ground motions

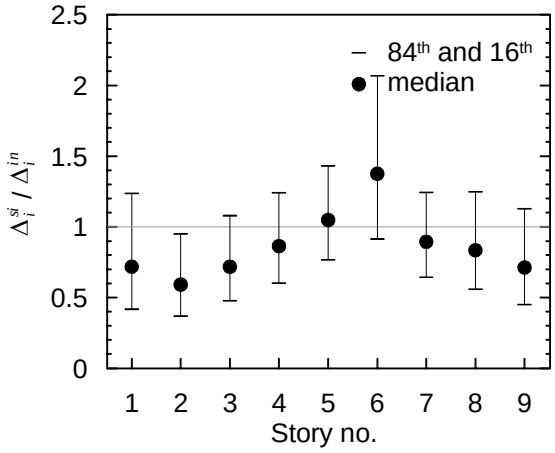

a. $\Delta_i^{si} / \Delta_i^{in}$ for M7 and NF motions

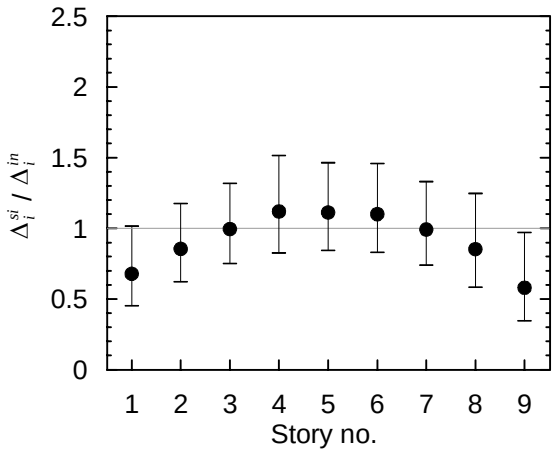

b. $\Delta_i^{si} / \Delta_i^{in}$ for M8 and NF motions

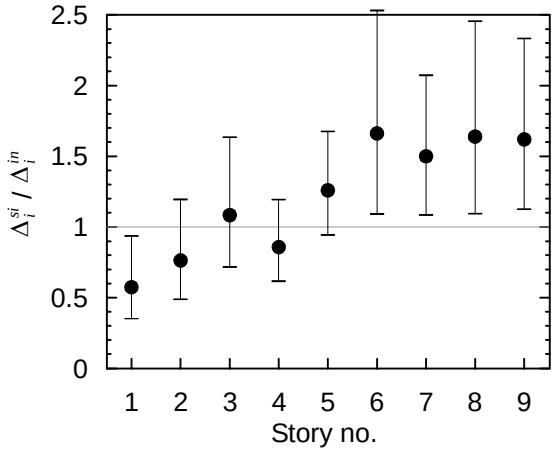

c. $\Delta_i^{si} / \Delta_i^{in}$ for M9 and NF motions

Figure 7. 84th, 50th and 16th percentiles of $\Delta_i^{si} / \Delta_i^{in}$ for nine-story models and NF ground motions

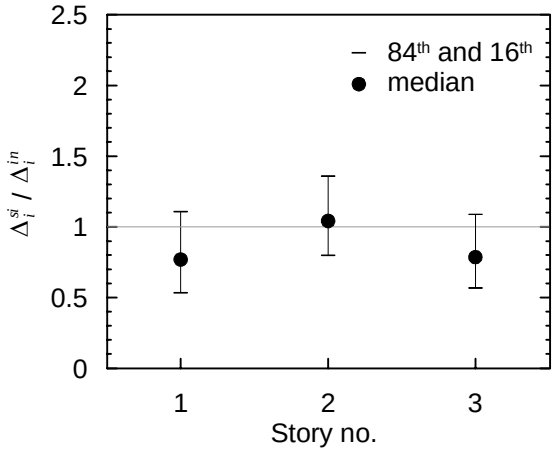

a. $\Delta_i^{si} / \Delta_i^{in}$ for M1 and FF motions

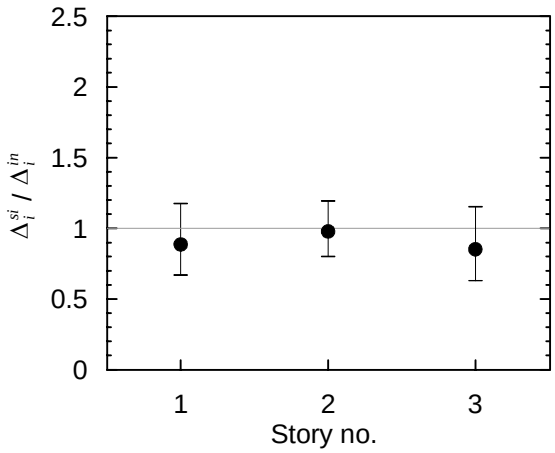

b. $\Delta_i^{si} / \Delta_i^{in}$ for M2 and FF motions

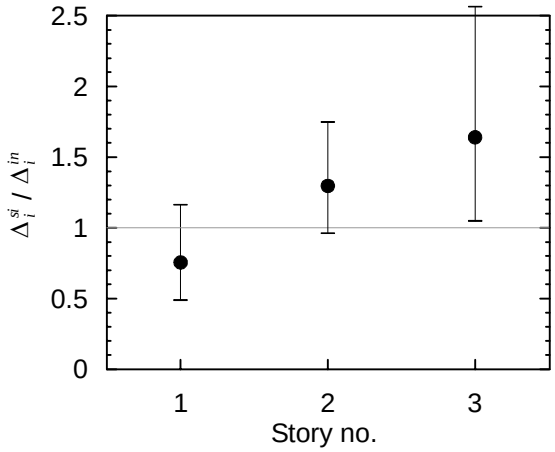

c. $\Delta_i^{si} / \Delta_i^{in}$ for M3 and FF motions

Figure 8. 84th, 50th and 16th percentiles of $\Delta_i^{si} / \Delta_i^{in}$ for three-story models and FF ground motions

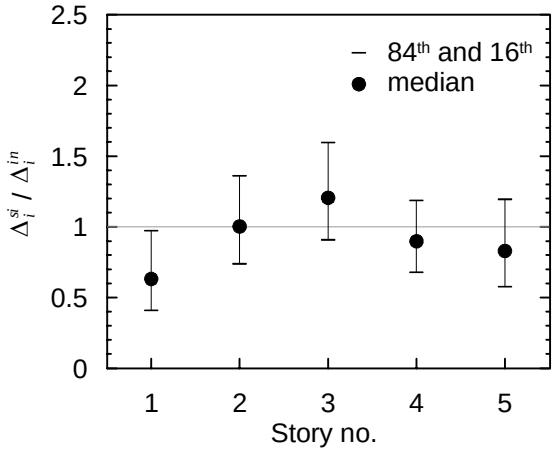

a. $\Delta_i^{si}/\Delta_i^{in}$ for M4 and FF motions

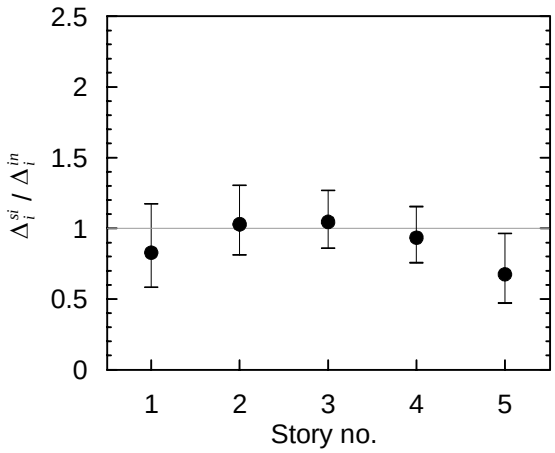

b. $\Delta_i^{si}/\Delta_i^{in}$ for M5 and FF motions

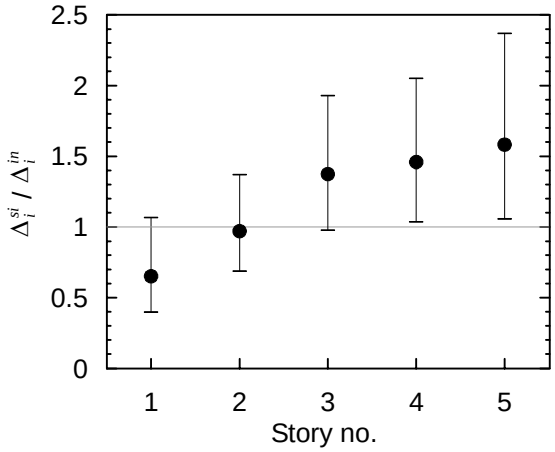

c. $\Delta_i^{si}/\Delta_i^{in}$ for M6 and FF motions

Figure 9. 84th, 50th and 16th percentiles of $\Delta_i^{si}/\Delta_i^{in}$ for five-story models and FF ground motions

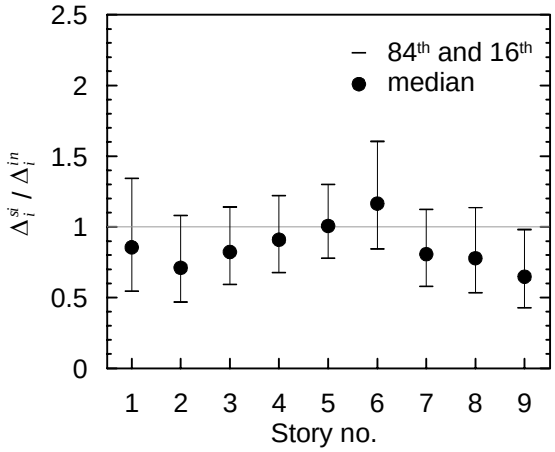

a. $\Delta_i^{si} / \Delta_i^{in}$ for M7 and FF motions

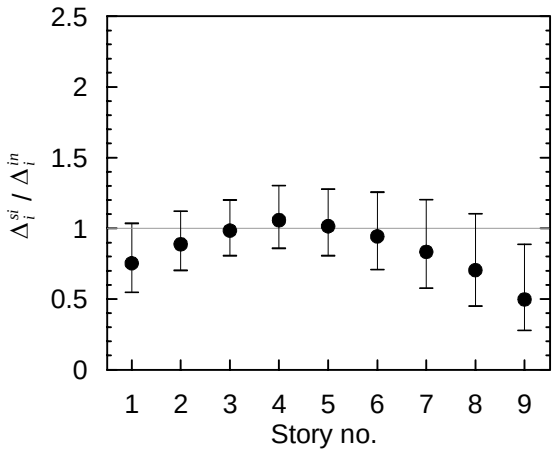

b. $\Delta_i^{si} / \Delta_i^{in}$ for M8 and FF motions

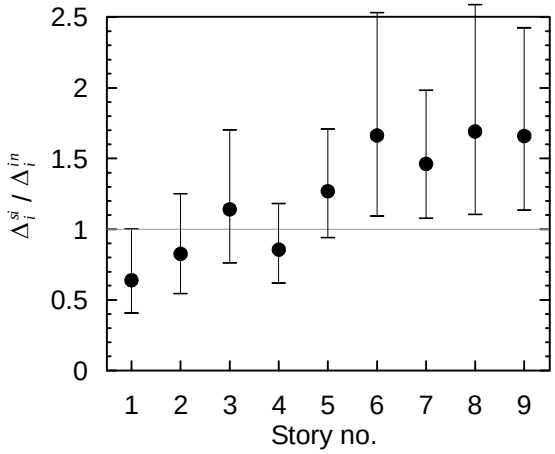

c. $\Delta_i^{si} / \Delta_i^{in}$ for M9 and FF motions

Figure 10. 84th, 50th and 16th percentiles of $\Delta_i^{si} / \Delta_i^{in}$ for nine-story models and FF ground motions

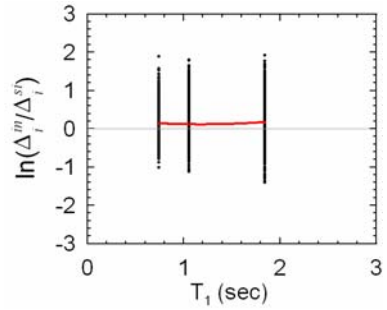

a. EBF, T_1

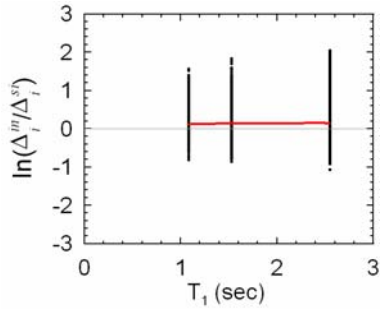

b. SMRF, T_1

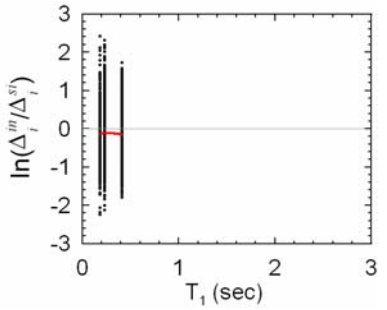

c. RCSW, T_1

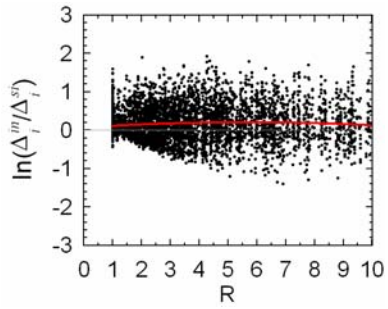

d. EBF, R

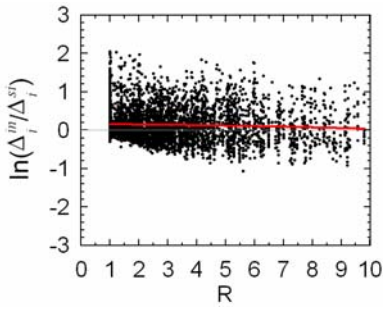

e. SMRF, R

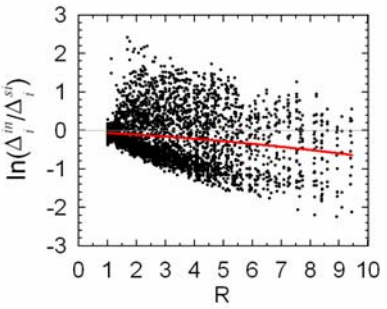

f. RCSW, R

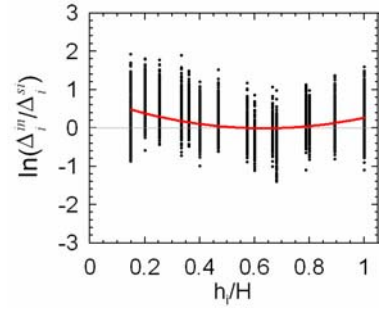

g. EBF, h_i/H

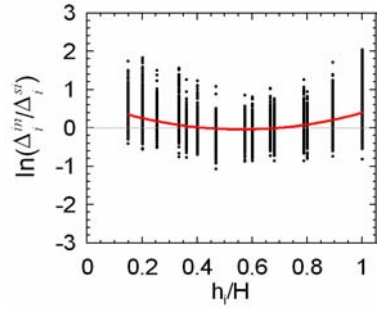

h. SMRF, h_i/H

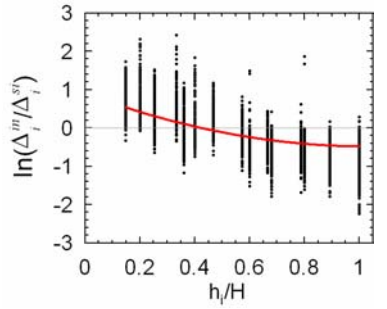

i. RCSW, h_i/H

Figure 11. $\Delta_i^{in}/\Delta_i^{si}$ **for EBF, SMRF and RCSW models as a function of** T_1, R and h_i/H

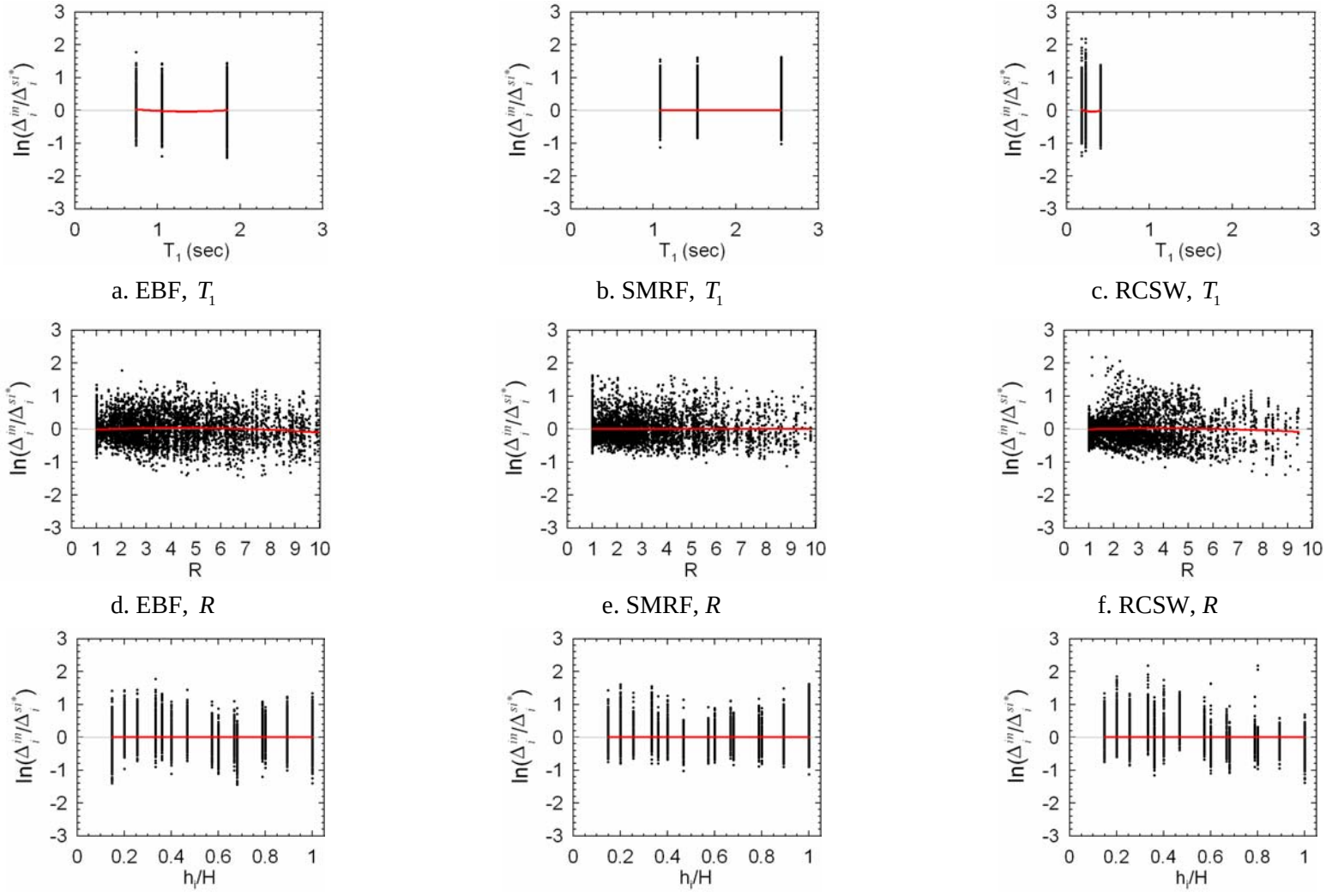

a. EBF, T_1 b. SMRF, T_1 c. RCSW, T_1

d. EBF, R e. SMRF, R f. RCSW, R

g. EBF, h_i/H h. SMRF, h_i/H i. RCSW, h_i/H

Figure 12. $\Delta_i^{in}/\Delta_i^{si*}$ **for EBF, SMRF and RCSW models as a function of** T_1, R and h_i/H

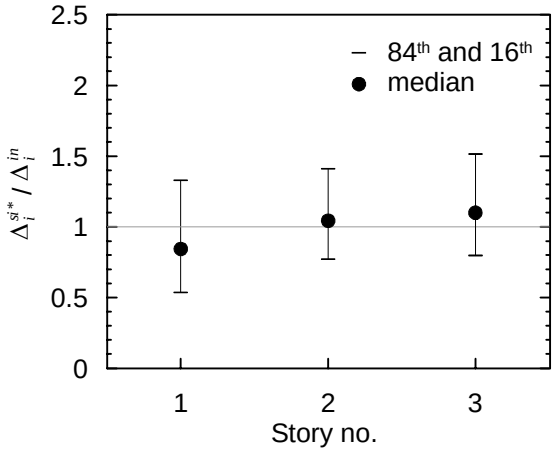

a. $\Delta_i^{si*}/\Delta_i^{in}$ for M1 and NF motions

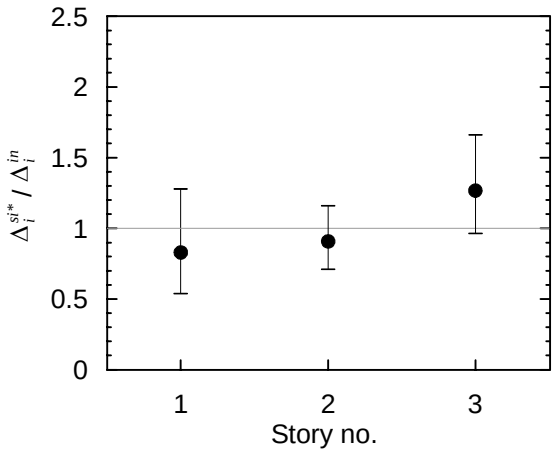

b. $\Delta_i^{si*}/\Delta_i^{in}$ for M2 and NF motions

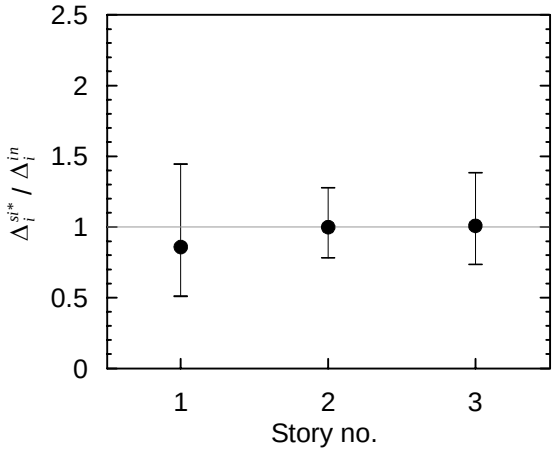

c. $\Delta_i^{si*}/\Delta_i^{in}$ for M3 and NF motions

Figure 13. 84th, 50th and 16th percentiles of $\Delta_i^{si*}/\Delta_i^{in}$ for three-story models and NF ground motions

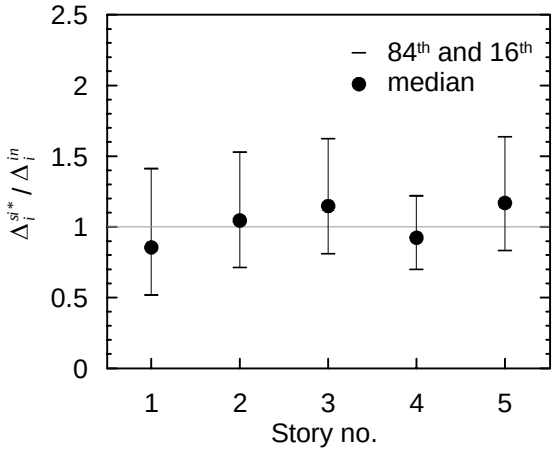

a. $\Delta_i^{si*}/\Delta_i^{in}$ for M4 and NF motions

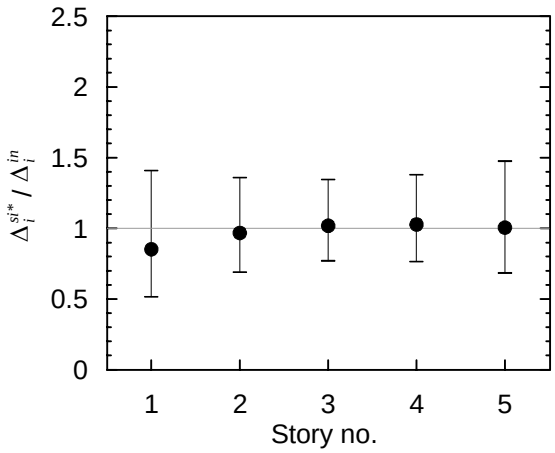

b. $\Delta_i^{si*}/\Delta_i^{in}$ for M5 and NF motions

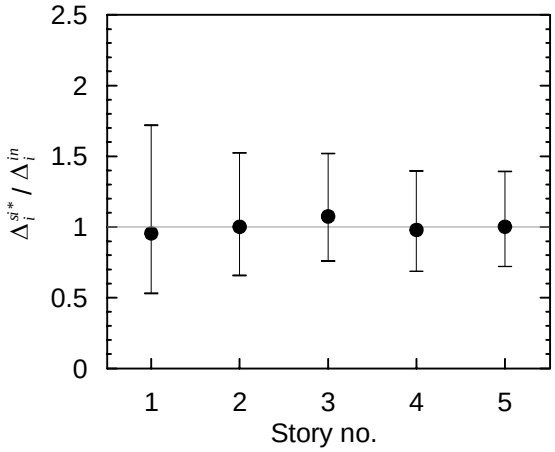

c. $\Delta_i^{si*}/\Delta_i^{in}$ for M6 and NF motions

Figure 14. 84th, 50th and 16th percentiles of $\Delta_i^{si*}/\Delta_i^{in}$ for five-story models and NF ground motions

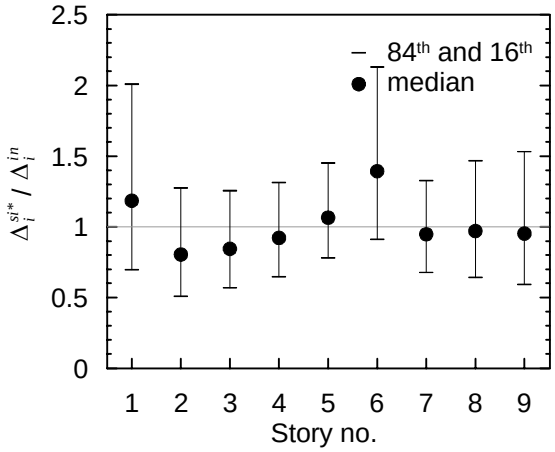

a. $\Delta_i^{si*}/\Delta_i^{in}$ for M7 and NF motions

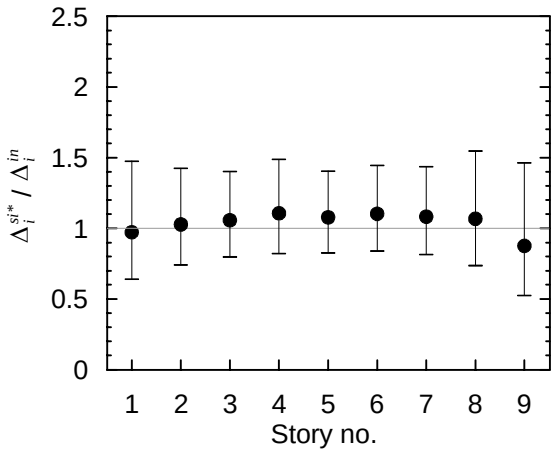

b. $\Delta_i^{si*}/\Delta_i^{in}$ for M8 and NF motions

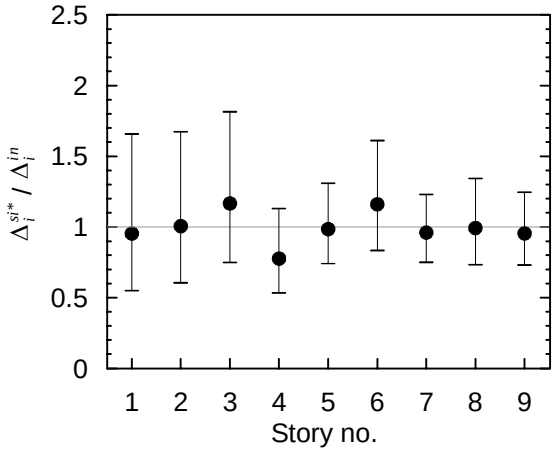

c. $\Delta_i^{si*}/\Delta_i^{in}$ for M9 and NF motions

Figure 15. 84th, 50th and 16th percentiles of $\Delta_i^{si*}/\Delta_i^{in}$ for nine-story models and NF ground motions

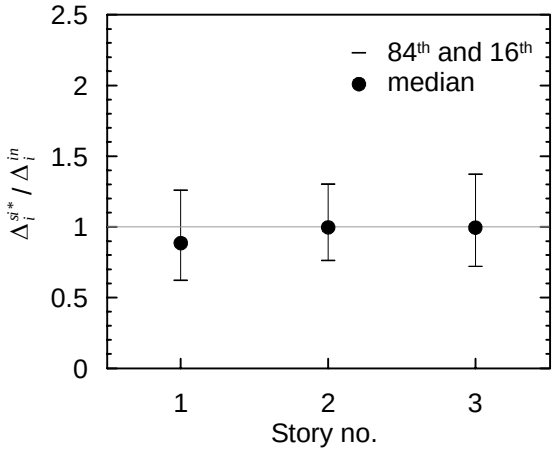

a. $\Delta_i^{si*}/\Delta_i^{in}$ for M1 and FF motions

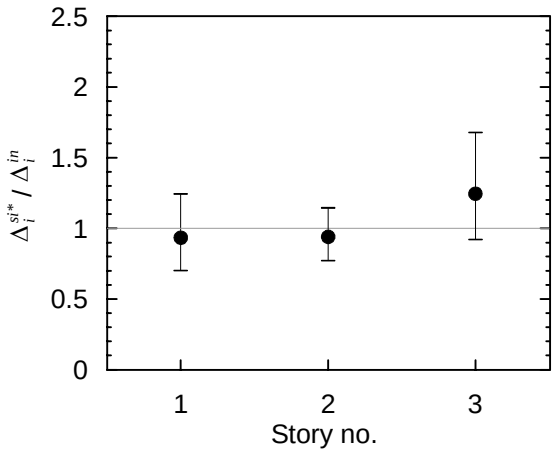

b. $\Delta_i^{si*}/\Delta_i^{in}$ for M2 and FF motions

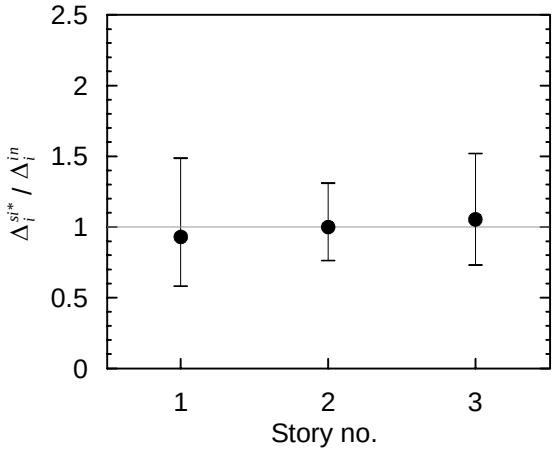

c. $\Delta_i^{si*}/\Delta_i^{in}$ for M3 and FF motions

Figure 16. 84th, 50th and 16th percentiles of $\Delta_i^{si*}/\Delta_i^{in}$ for three-story models and FF ground motions

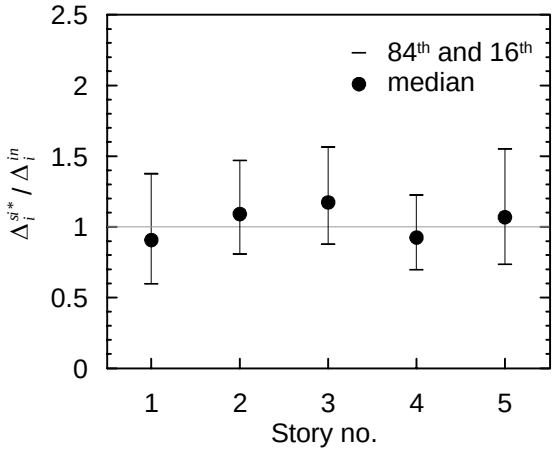

a. $\Delta_i^{si*}/\Delta_i^{in}$ for M4 and FF motions

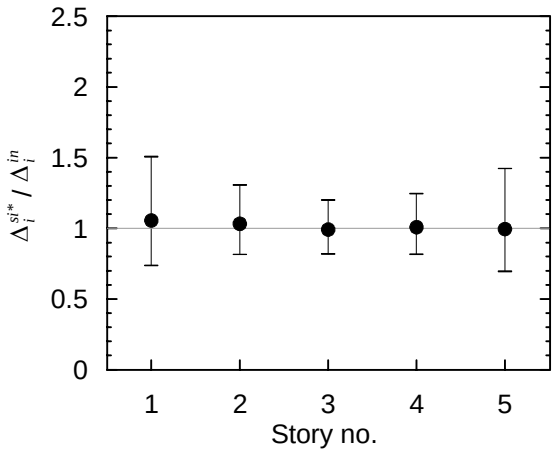

b. $\Delta_i^{si*}/\Delta_i^{in}$ for M5 and FF motions

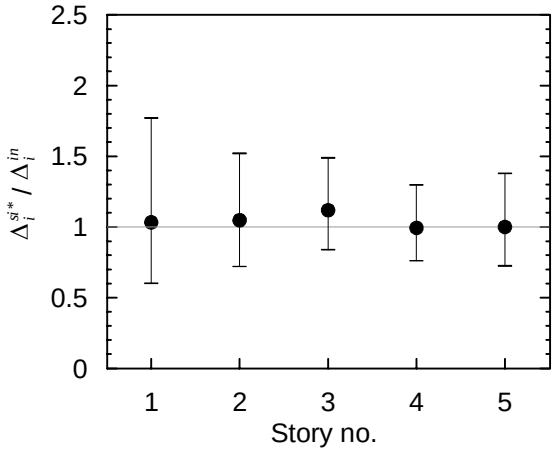

c. $\Delta_i^{si*}/\Delta_i^{in}$ for M6 and FF motions

Figure 17. 84th, 50th and 16th percentiles of $\Delta_i^{si*}/\Delta_i^{in}$ for five-story models and FF ground motions

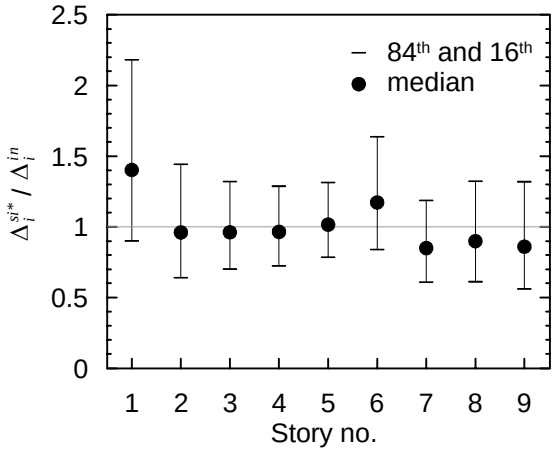

a. $\Delta_i^{si*}/\Delta_i^{in}$ for M7 and FF motions

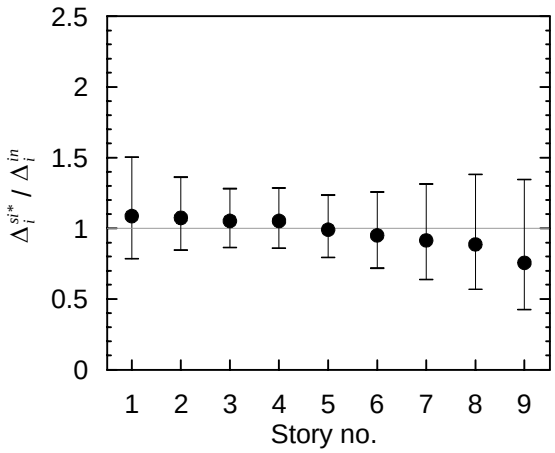

b. $\Delta_i^{si*}/\Delta_i^{in}$ for M8 and FF motions

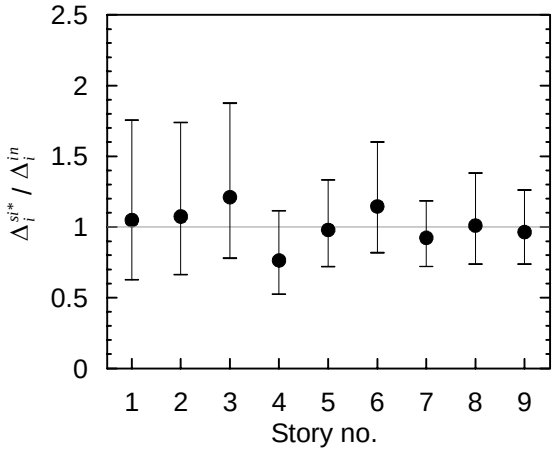

c. $\Delta_i^{si*}/\Delta_i^{in}$ for M9 and FF motions

Figure 18. 84th, 50th and 16th percentiles of $\Delta_i^{si*}/\Delta_i^{in}$ for nine-story models and FF ground motions

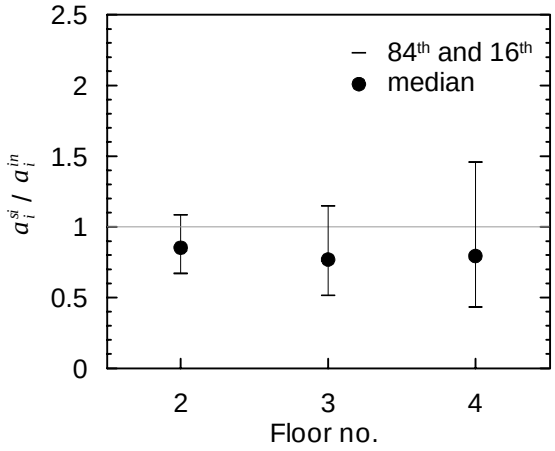

a. a_i^{si} / a_i^{in} for M1 and NF motions

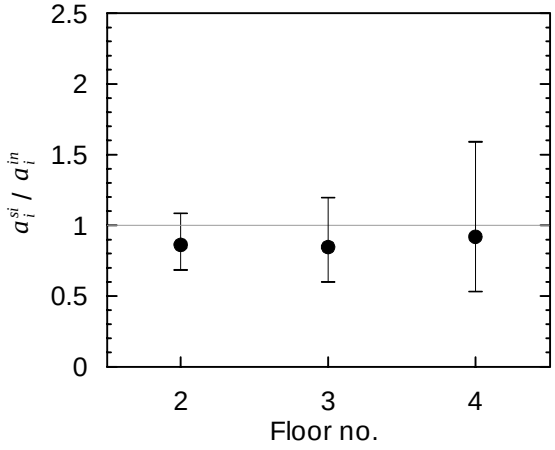

b. a_i^{si} / a_i^{in} for M2 and NF motions

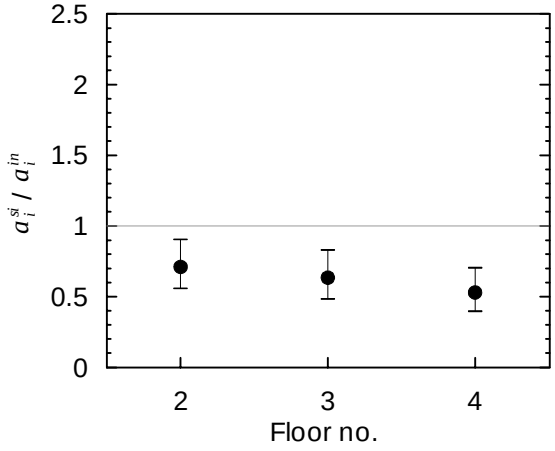

c. a_i^{si} / a_i^{in} for M3 and NF motions

Figure 19. 84th, 50th and 16th percentiles of a_i^{si} / a_i^{in} for three-story models and NF ground motions

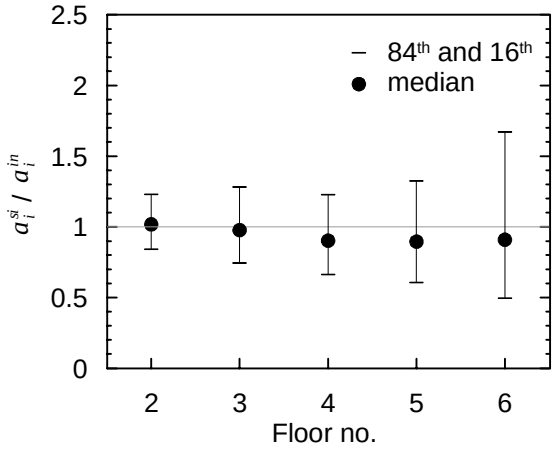

a. a_i^{si} / a_i^{in} for M4 and NF motions

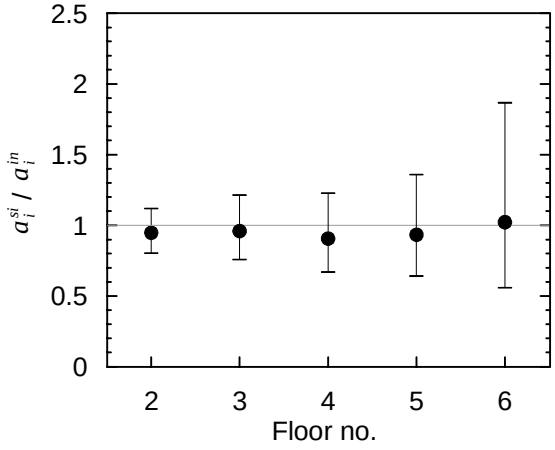

b. a_i^{si} / a_i^{in} for M5 and NF motions

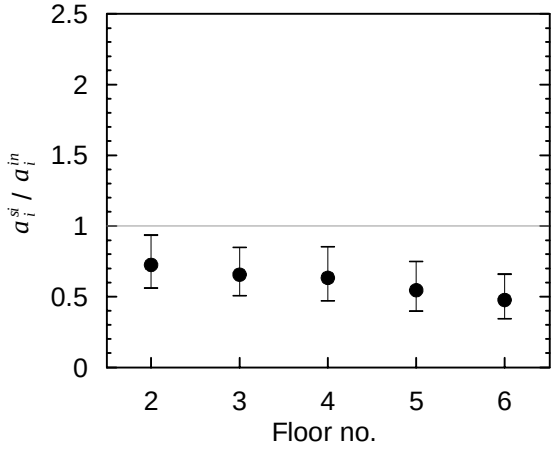

c. a_i^{si} / a_i^{in} for M6 and NF motions

Figure 20. 84th, 50th and 16th percentiles of a_i^{si} / a_i^{in} for five-story models and NF ground motions

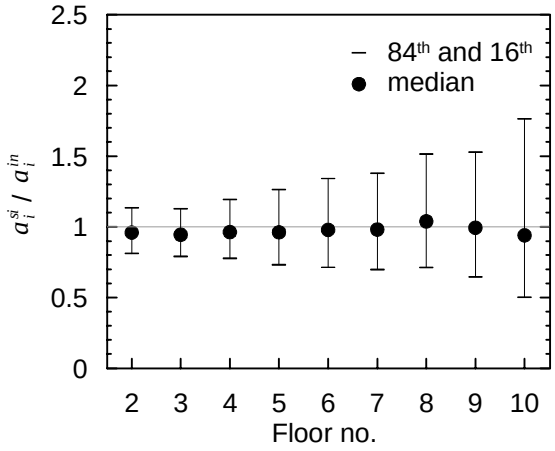

a. a_i^{si} / a_i^{in} for M7 and NF motions

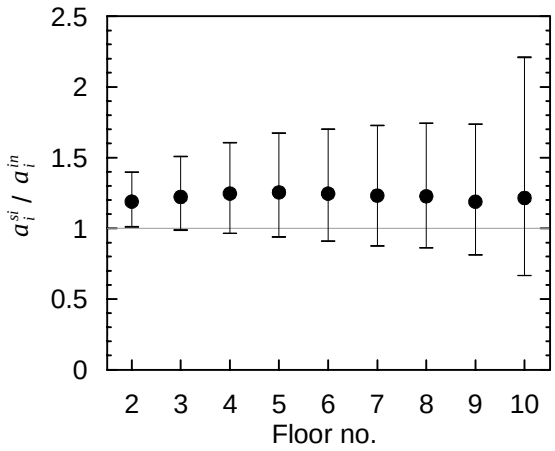

b. a_i^{si} / a_i^{in} for M8 and NF motions

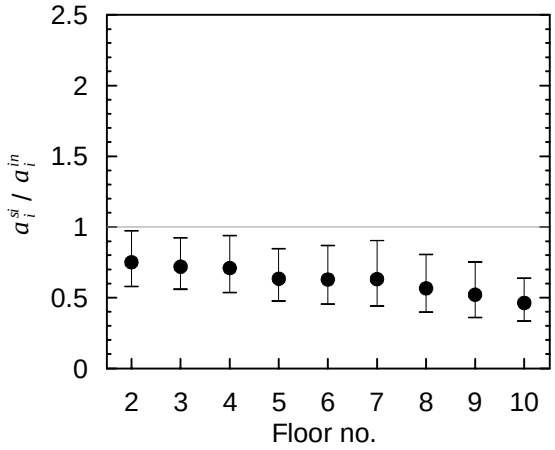

c. a_i^{si} / a_i^{in} for M9 and NF motions

Figure 21. 84th, 50th and 16th percentiles of a_i^{si} / a_i^{in} for nine-story models and NF ground motions

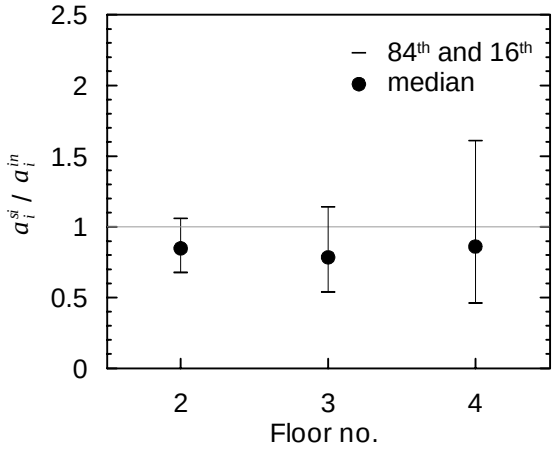

a. a_i^{si} / a_i^{in} for M1 and FF motions

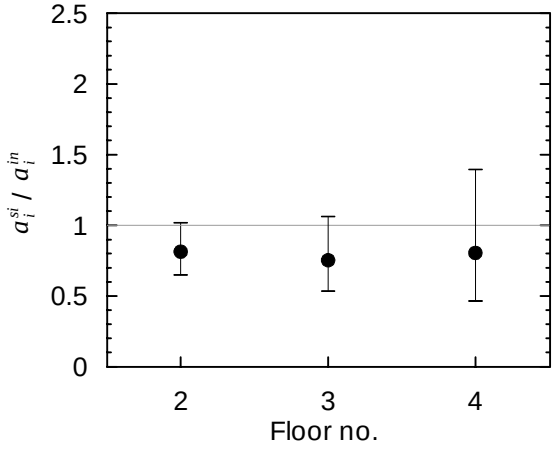

b. a_i^{si} / a_i^{in} for M2 and FF motions

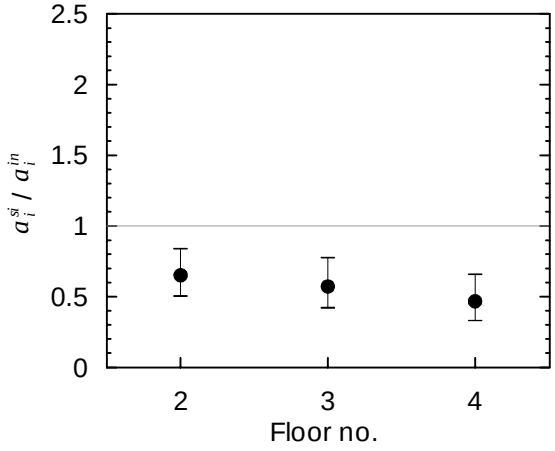

c. a_i^{si} / a_i^{in} for M3 and FF motions

Figure 22. 84th, 50th and 16th percentiles of a_i^{si} / a_i^{in} for three-story models and FF ground motions

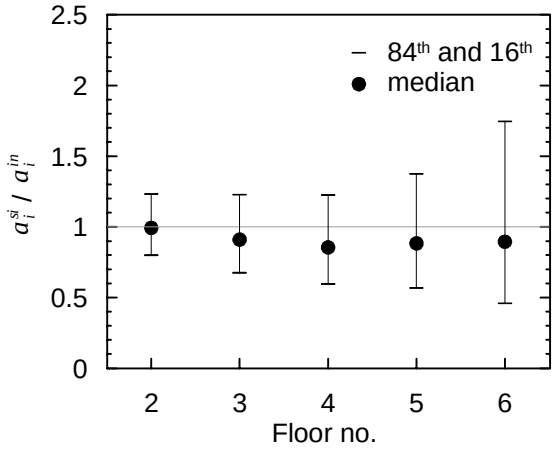

a. a_i^{si} / a_i^{in} for M4 and FF motions

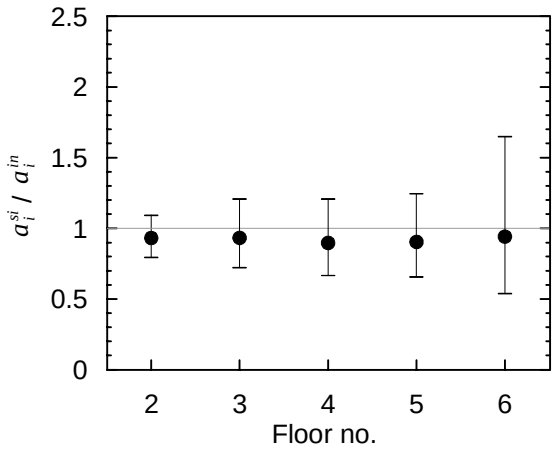

b. a_i^{si} / a_i^{in} for M5 and FF motions

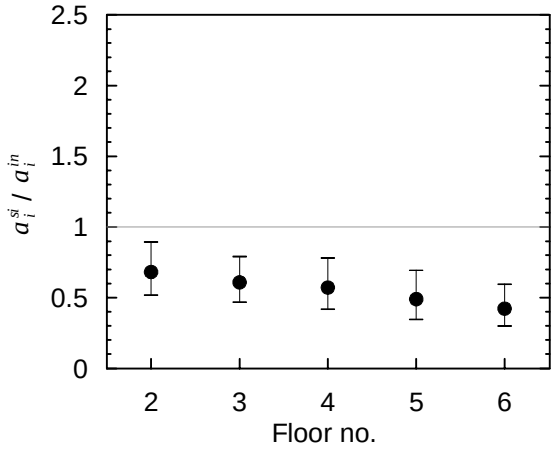

c. a_i^{si} / a_i^{in} for M6 and FF motions

Figure 23. 84th, 50th and 16th percentiles of a_i^{si} / a_i^{in} for five-story models and FF ground motions

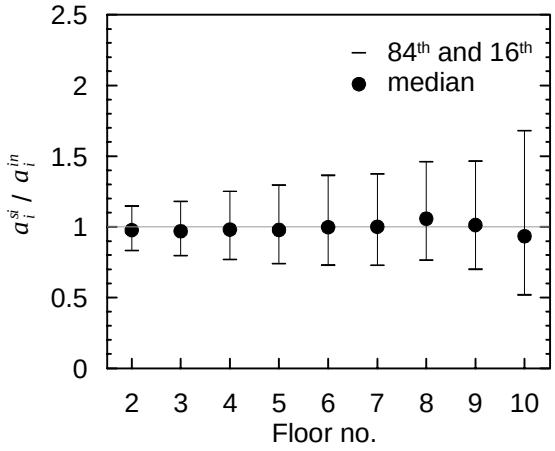

a. a_i^{si} / a_i^{in} for M7 and FF motions

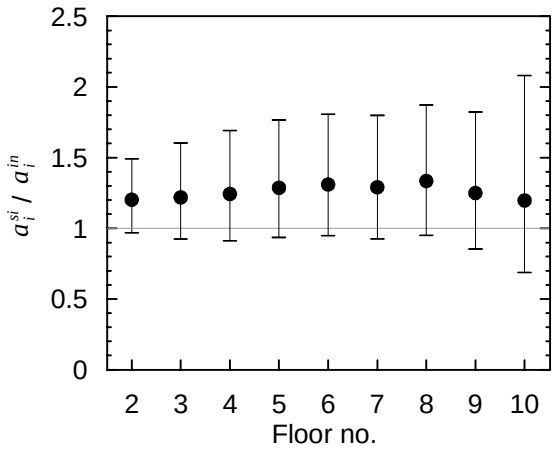

b. a_i^{si} / a_i^{in} for M8 and FF motions

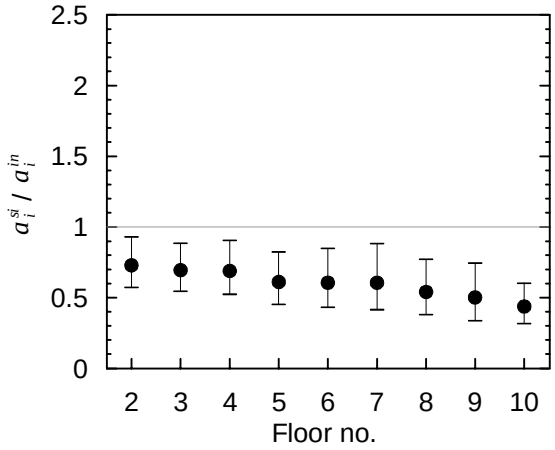

c. a_i^{si} / a_i^{in} for M9 and FF motions

Figure 24. 84th, 50th and 16th percentiles of a_i^{si} / a_i^{in} for nine-story models and FF ground motions

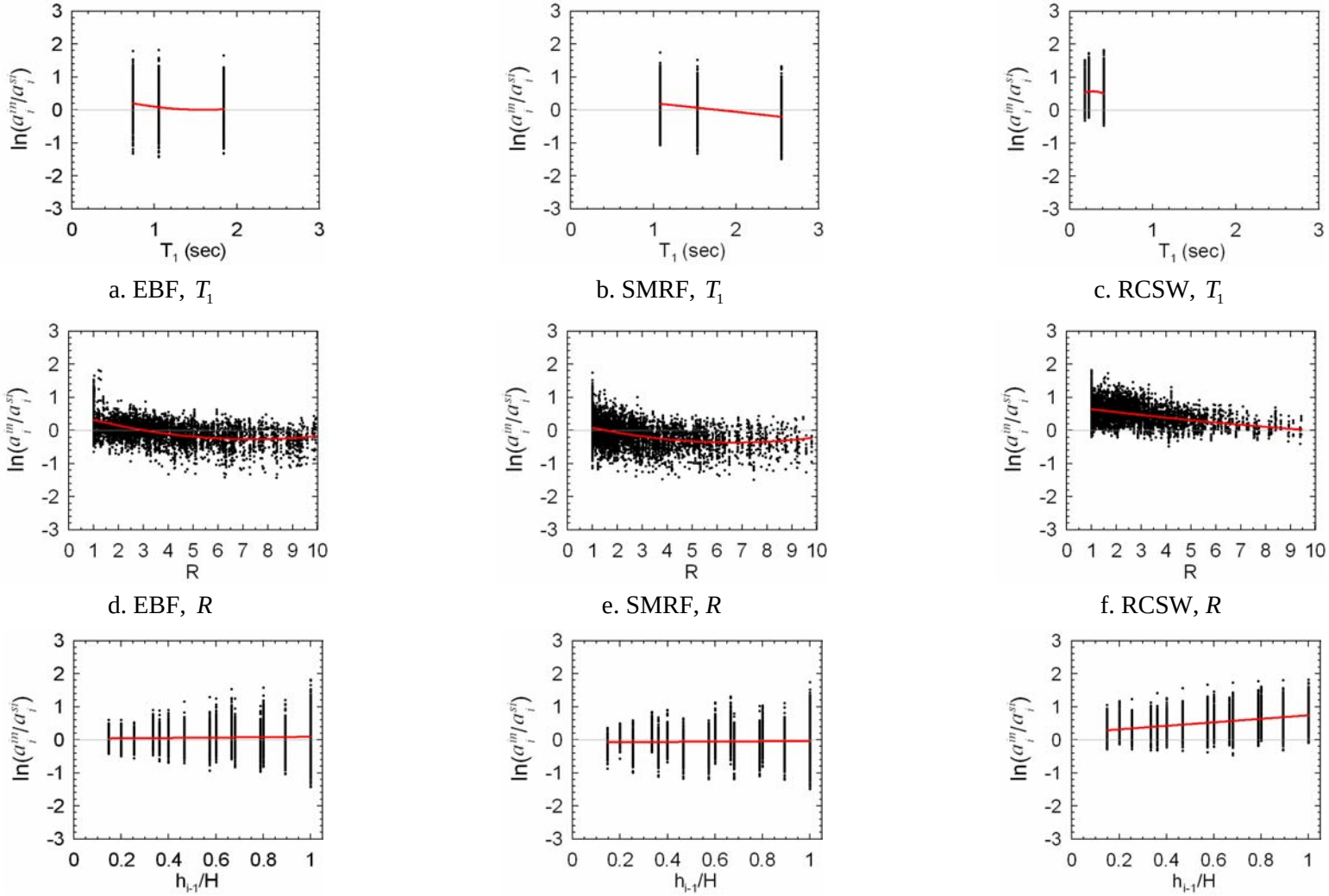

a. EBF, T_1 b. SMRF, T_1 c. RCSW, T_1

d. EBF, R e. SMRF, R f. RCSW, R

g. EBF, h_{i-1}/H h. SMRF, h_{i-1}/H i. RCSW, h_{i-1}/H

Figure 25. a_i^{in}/a_i^{si} **for EBF, SMRF and RCSW models as a function of** T_1, R and h_{i-1}/H

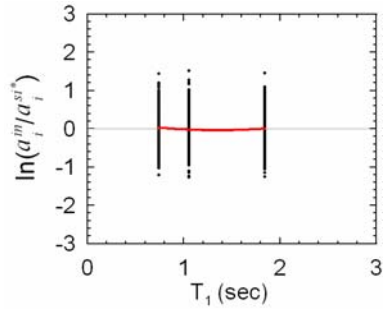

a. EBF, T_1

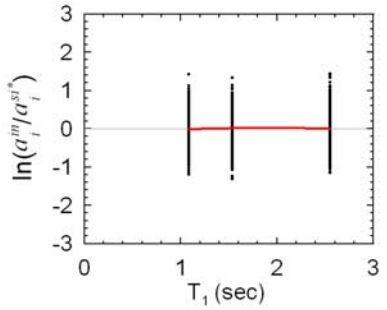

b. SMRF, T_1

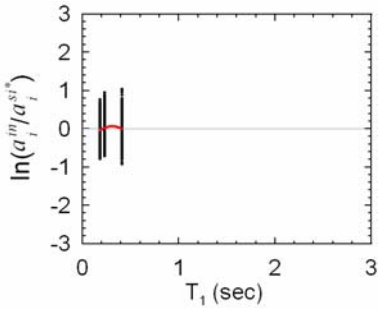

c. RCSW, T_1

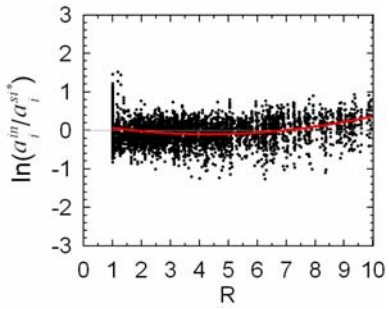

d. EBF, R

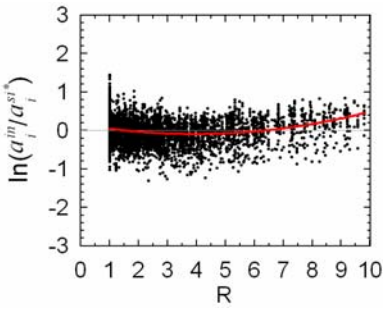

e. SMRF, R

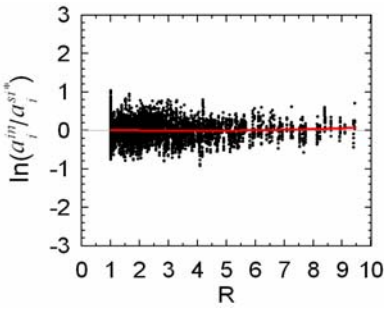

f. RCSW, R

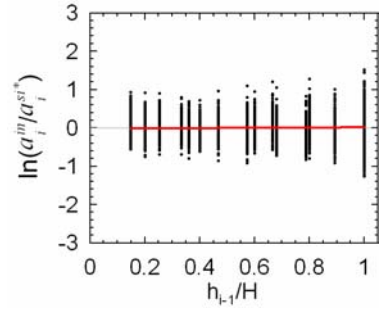

g. EBF, h_{i-1}/H

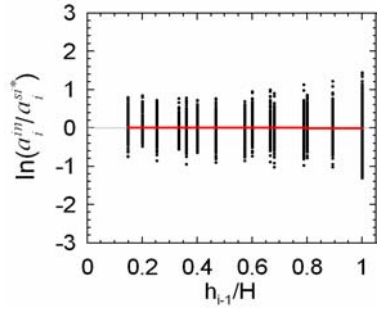

h. SMRF, h_{i-1}/H

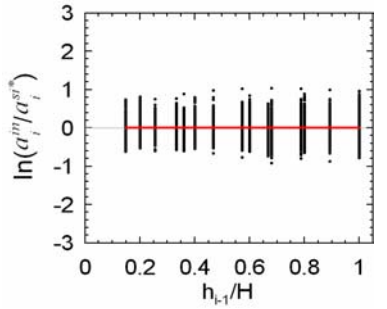

i. RCSW, h_{i-1}/H

Figure 26. a_i^{in}/a_i^{si*} **for EBF, SMRF and RCSW models as a function of** T_1, R and h_{i-1}/H

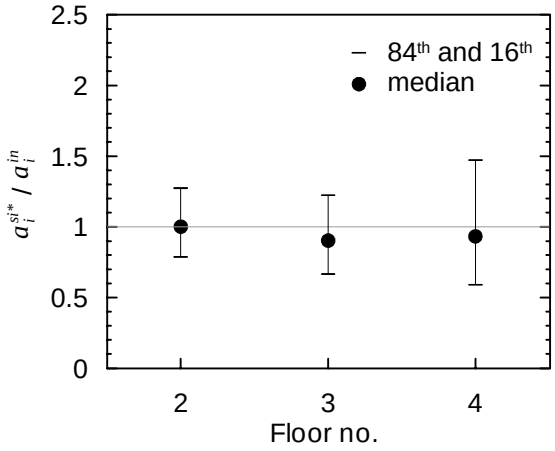

a. a_i^{si*}/a_i^{in} for M1 and NF motions

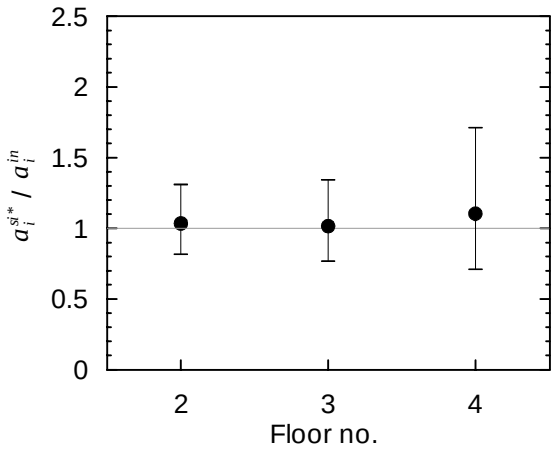

b. a_i^{si*}/a_i^{in} for M2 and NF motions

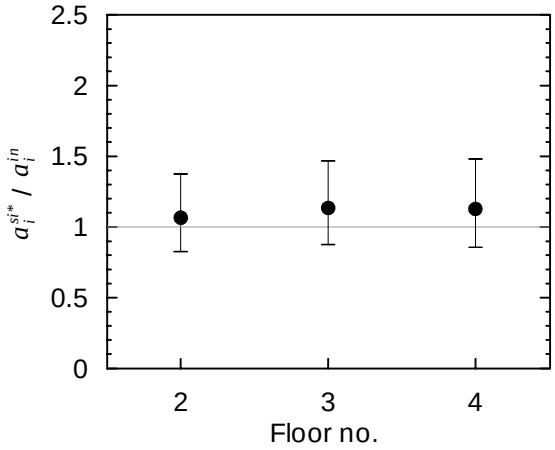

c. a_i^{si*}/a_i^{in} for M3 and NF motions

Figure 27. 84th, 50th and 16th percentiles of a_i^{si*}/a_i^{in} for three-story models and NF ground motions

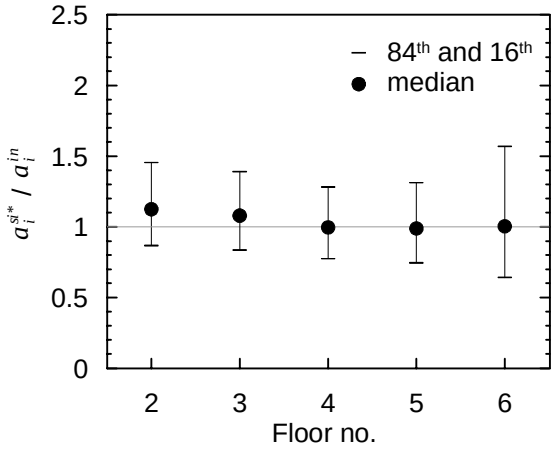

a. a_i^{si*}/a_i^{in} for M4 and NF motions

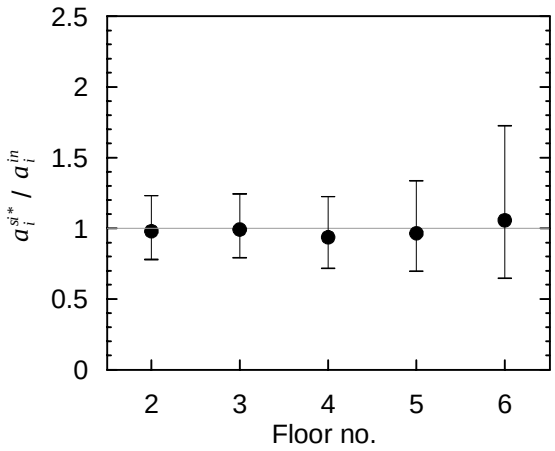

b. a_i^{si*}/a_i^{in} for M5 and NF motions

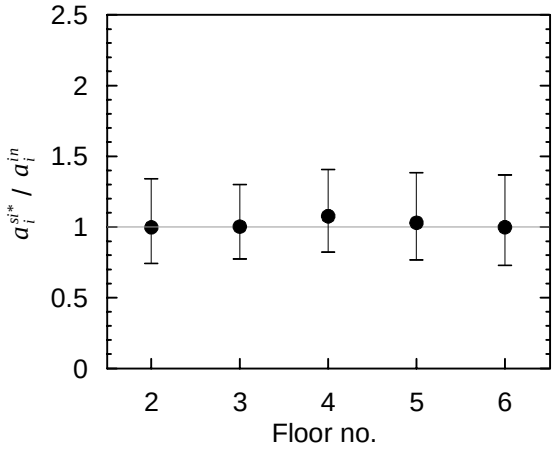

c. a_i^{si*}/a_i^{in} for M6 and NF motions

Figure 28. 84th, 50th and 16th percentiles of a_i^{si*}/a_i^{in} for five-story models and NF ground motions

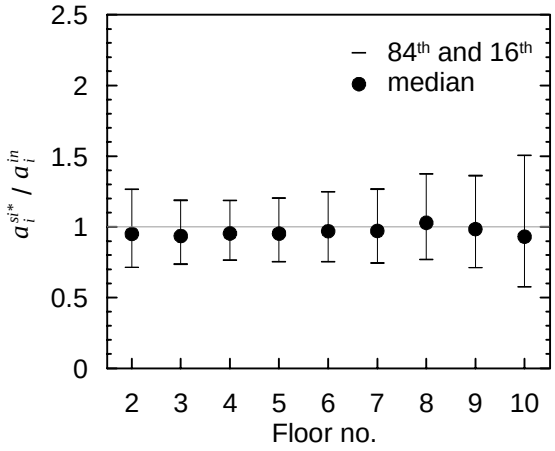

a. a_i^{si*}/a_i^{in} for M7 and NF motions

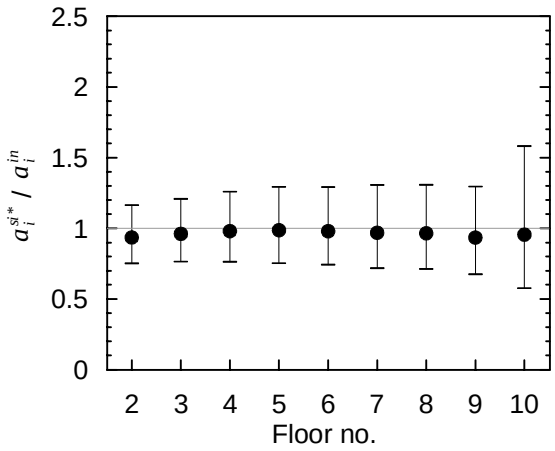

b. a_i^{si*}/a_i^{in} for M8 and NF motions

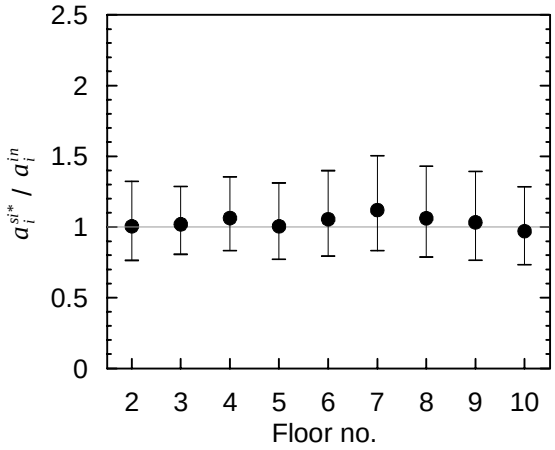

c. a_i^{si*}/a_i^{in} for M9 and NF motions

Figure 29. 84th, 50th and 16th percentiles of a_i^{si*}/a_i^{in} for nine-story models and NF ground motions

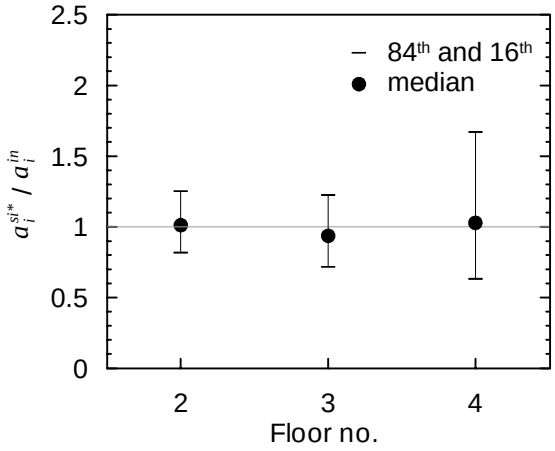

a. a_i^{si*}/a_i^{in} for M1 and FF motions

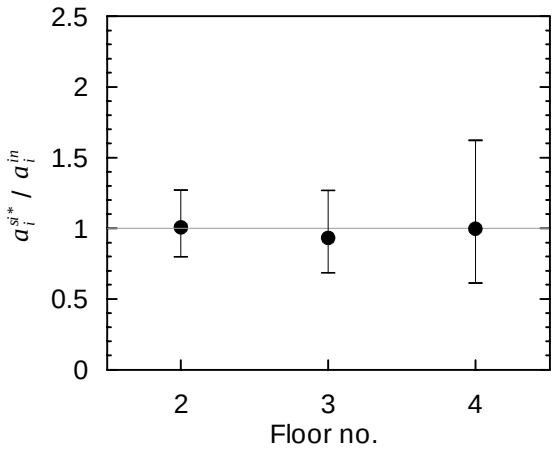

b. a_i^{si*}/a_i^{in} for M2 and FF motions

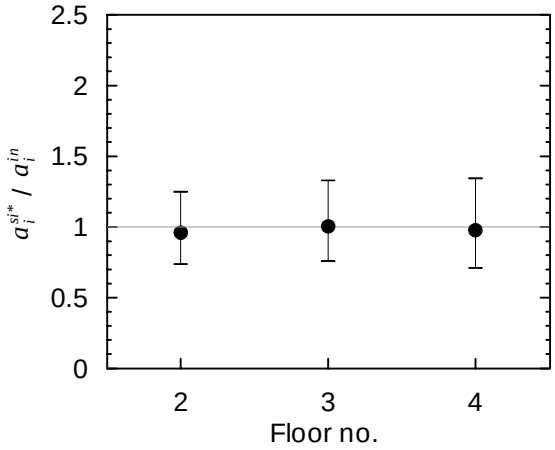

c. a_i^{si*}/a_i^{in} for M3 and FF motions

Figure 30. 84th, 50th and 16th percentiles of a_i^{si*}/a_i^{in} for three-story models and FF ground motions

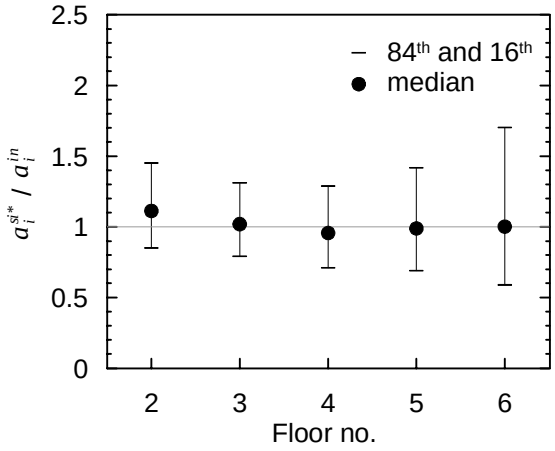

a. a_i^{si*}/a_i^{in} for M4 and FF motions

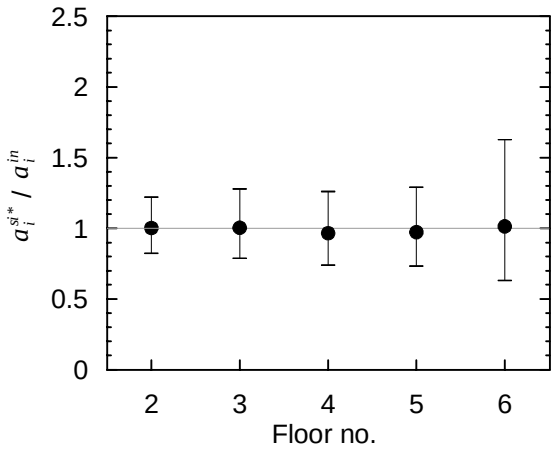

b. a_i^{si*}/a_i^{in} for M5 and FF motions

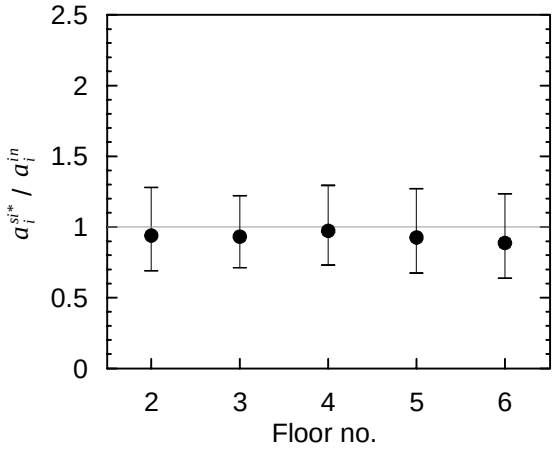

c. a_i^{si*}/a_i^{in} for M6 and FF motions

Figure 31. 84th, 50th and 16th percentiles of a_i^{si*}/a_i^{in} for five-story models and FF ground motions

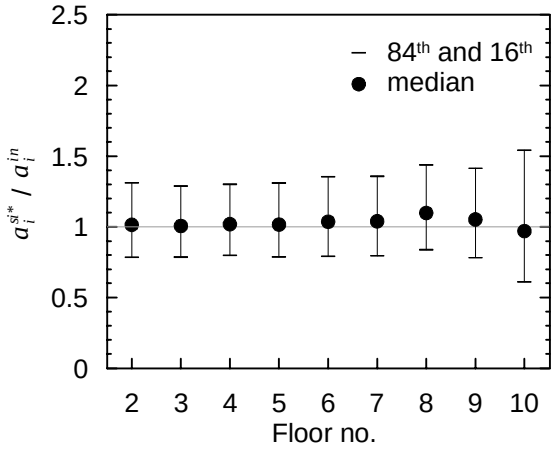

a. a_i^{si*}/a_i^{in} for M7 and FF motions

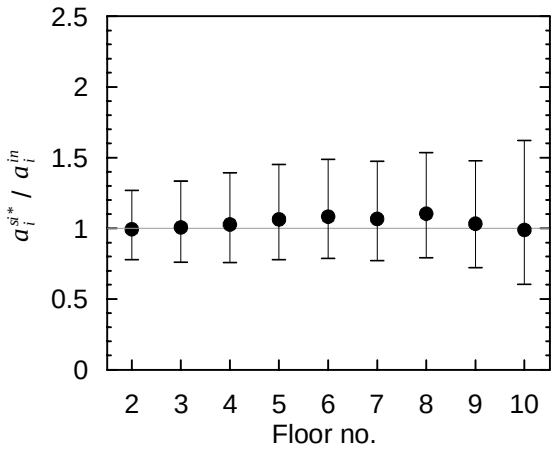

b. a_i^{si*}/a_i^{in} for M8 and FF motions

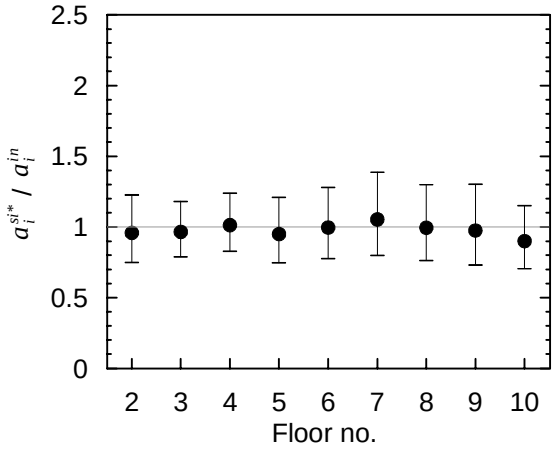

c. a_i^{si*}/a_i^{in} for M9 and FF motions

Figure 32. 84th, 50th and 16th percentiles of a_i^{si*}/a_i^{in} for nine-story models and FF ground motions